nature portfolio

https://doi.org/10.1038/s41596-021-00587-1

Supplementary information

Hierarchical imaging and computational analysis of three-dimensional vascular network architecture in the entire postnatal and adult mouse brain

In the format provided by the authors and unedited

SUPPLEMENTARY FIGURES

Supplementary Figure 1

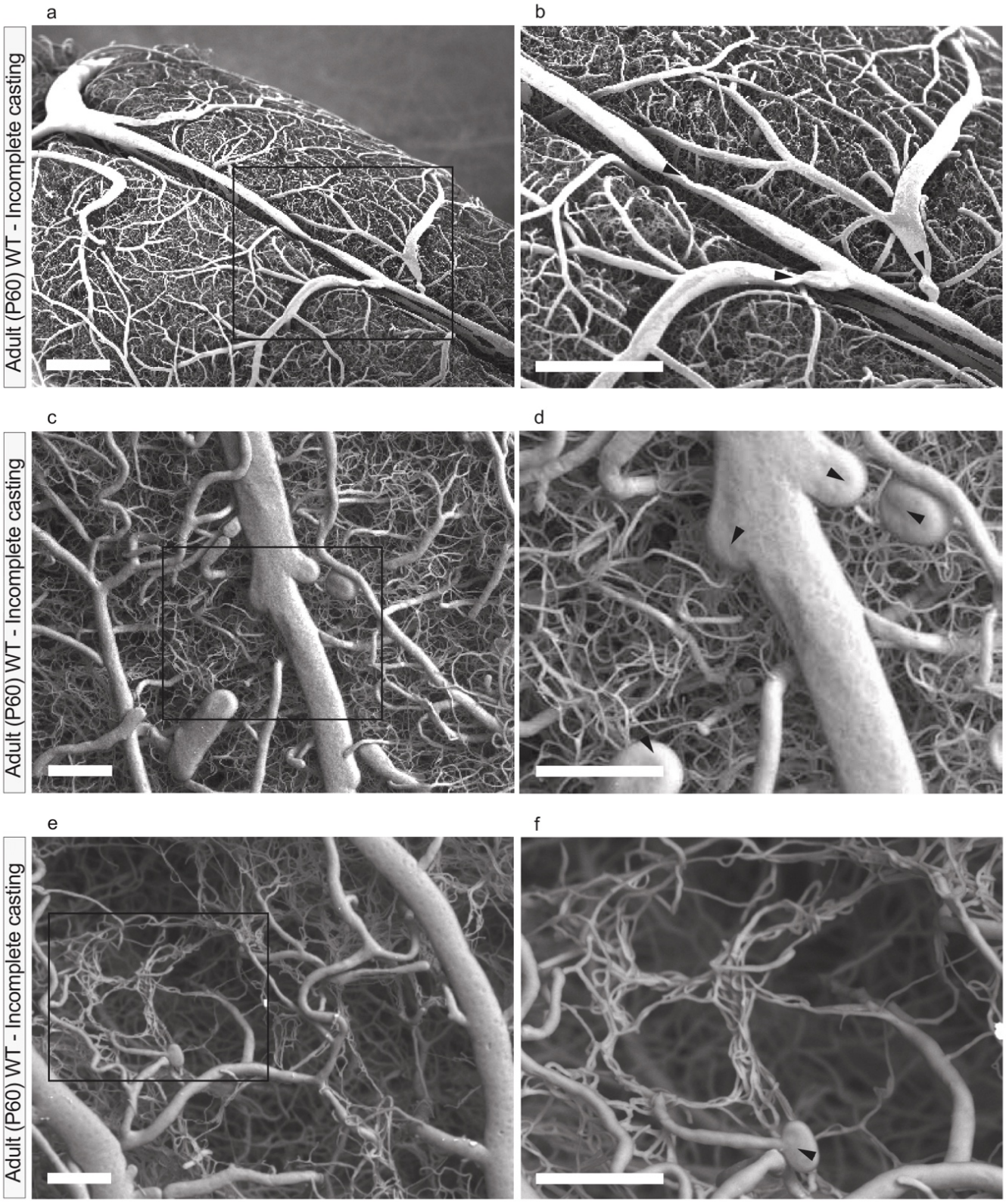

Supplementary Figure 1 Validation of vascular corrosion casting in adult (P60) mice using scanning electron microscopy (SEM) – examples of insufficiently perfused mouse brain vasculature

Quality control of the vascular corrosion casts of P60 WT mice by SEM. **a**,**b** SEM images showing the cortical surface of a vascular corrosion cast illustrating abrupt changes in segment diameter (arrowheads), likely caused by vessel lumen obstruction during resin perfusion. **c**,**d** The irregular surface shape of vessels combined with rounded abrupt ends of larger vessels are the typical signs of incomplete vascular corrosion casting. The rounded abrupt dead-ends (arrowheads) are caused by casting material pushing against trapped air pockets that were introduced during the perfusion procedure, thereby interrupting physiological flow. Absence of imprints of endothelial cell nuclei further indicates insufficient casting. **e**,**f** Larger vessels are visibly distended with rounded abrupt dead-ends (arrowheads) and are missing endothelial cell nuclei imprints. The capillary network in the cortex is not well defined and shows interruptions, further illustrating incomplete casting. Scale bars: 200 μm (**a**); 200 μm (**b**); 150 μm (**c**); 150 μm (**d**), 150 μm (**e**), 150 μm (**f**).

Supplementary Figure 2

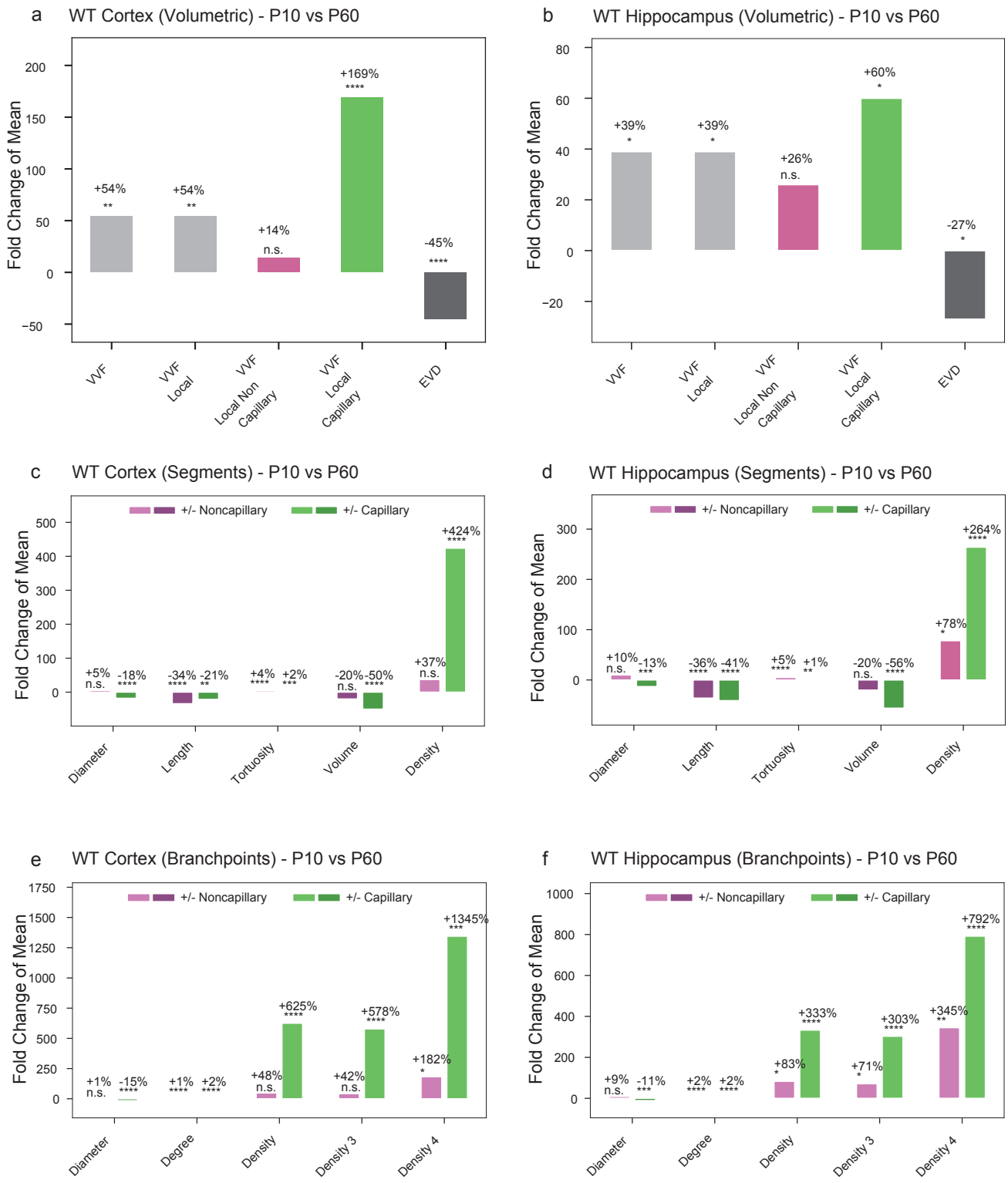

Supplementary Figure 2 Overview of the main vascular parameters in various regions of the wildtype postnatal and adult mouse brain

Quantification of the main vascular parameters, depicted as fold change of the mean in the WT P60 mouse brain as compared to the P10 mouse brain. **a**,**b**,**g** On a volumetric level, the vascular volume fraction (VVF), was analyzed by computational analysis using the global morphometry, and local topology approach in the cortex (**a**), hippocampus (**b**) and superior colliculus (**g**). The vascular volume fraction in all these brain structures was significantly higher in the WT P60 animals than that in the P10 WT animals. **c**,**d**,**h** On the level of vascular segments, the parameters segment diameter, length, tortuosity, volume and density are depicted as fold change of the mean. The parameters segment diameter, length and volume show a highly significant decrease or nonsignificant increase, whereas the parameters segment tortuosity and density show an increase. All these changes are most pronounced on the capillary level. **e**,**f**,**i** Investigating the difference in branchpoint characteristics between P60 and P10 wildtype mouse brains, the vascular parameters branch point diameter, degree, density, branch point degree 3 density and branch point degree 4 density were analyzed. Branch point diameter shows a significant decrease in the P60 as compared to the P10 mouse brain on a capillary level in all three brain regions. The vascular parameters branch point degree, density, branch point degree 3 density and branch point degree 4 density all show a relative increase, again most pronounced on the capillary level, in all three brain regions (n = 4-6 for P10 WT; n = 8-12 for P60 WT; n = 3-5 for P10 Nogo-A$^{-/-}$; n = 8-11 for P60 Nogo-A$^{-/-}$ animals; and in average three ROIs per animal and brain region were used). All data are shown as fold change of the mean distributions, where the magenta bars correspond to the noncapillaries and the green bar corresponds to the capillaries. *$P < 0.05$, **$P < 0.01$, ***$P < 0.001$.

Supplementary Figure 3

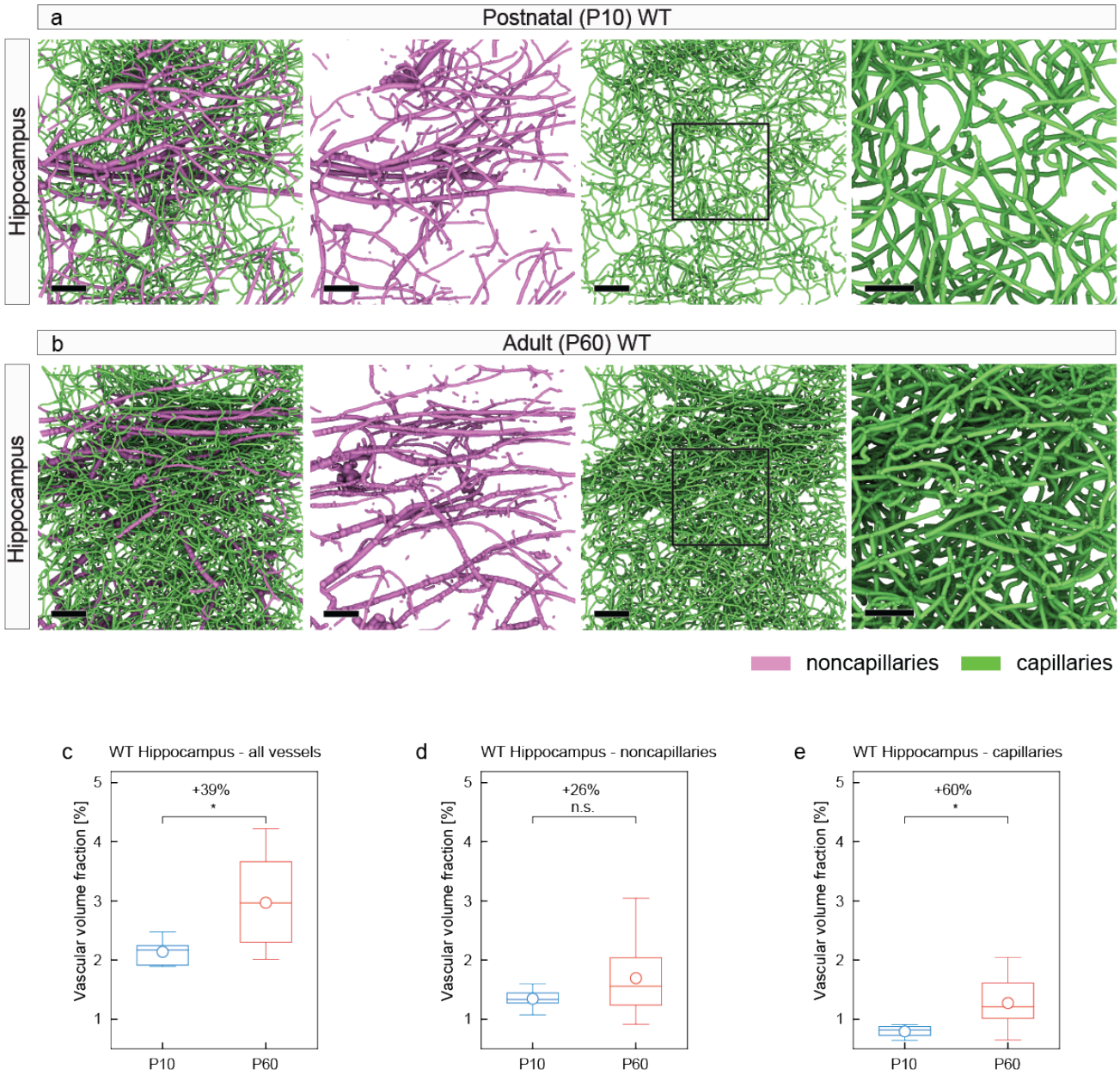

Supplementary Figure 3 Local vascular network topology – Increased vascular volume fraction of the adult (P60) WT versus postnatal (P10) WT hippocampi mainly found at the capillary level

a,**b** Three-dimensional computational reconstruction of µCT scans of vascular networks in the hippocampus of a P60 WT sample highlighting a vessel tree with noncapillaries in magenta and capillaries in green. **c-e** Quantification of the 3D vascular volume fraction for all vessels (**c**), noncapillaries (**d**), and capillaries (**e**) in P10 WT and P60 WT calculated by local topology analysis. The significant increase of the vascular volume

fraction for all vessels in the P60 WT animals (**c**) was mainly due to a significant increase at the level of capillaries (**e**) (n = 4-6 for P10 WT; n = 8-12 for P60 WT animals were used; and in average three ROIs per animal and brain region were used). All data are shown as mean distributions where the open dot represents the mean. Boxplots indicate the 25% to 75% quartiles of the data. The shaded blue and red areas indicate the SD. **P* < 0.05, ***P* < 0.01, ****P* < 0.001. Scale bars: 100 µm (**a**,**b**, overviews); 50 µm (**a**,**b**, zooms).

Supplementary Figure 4

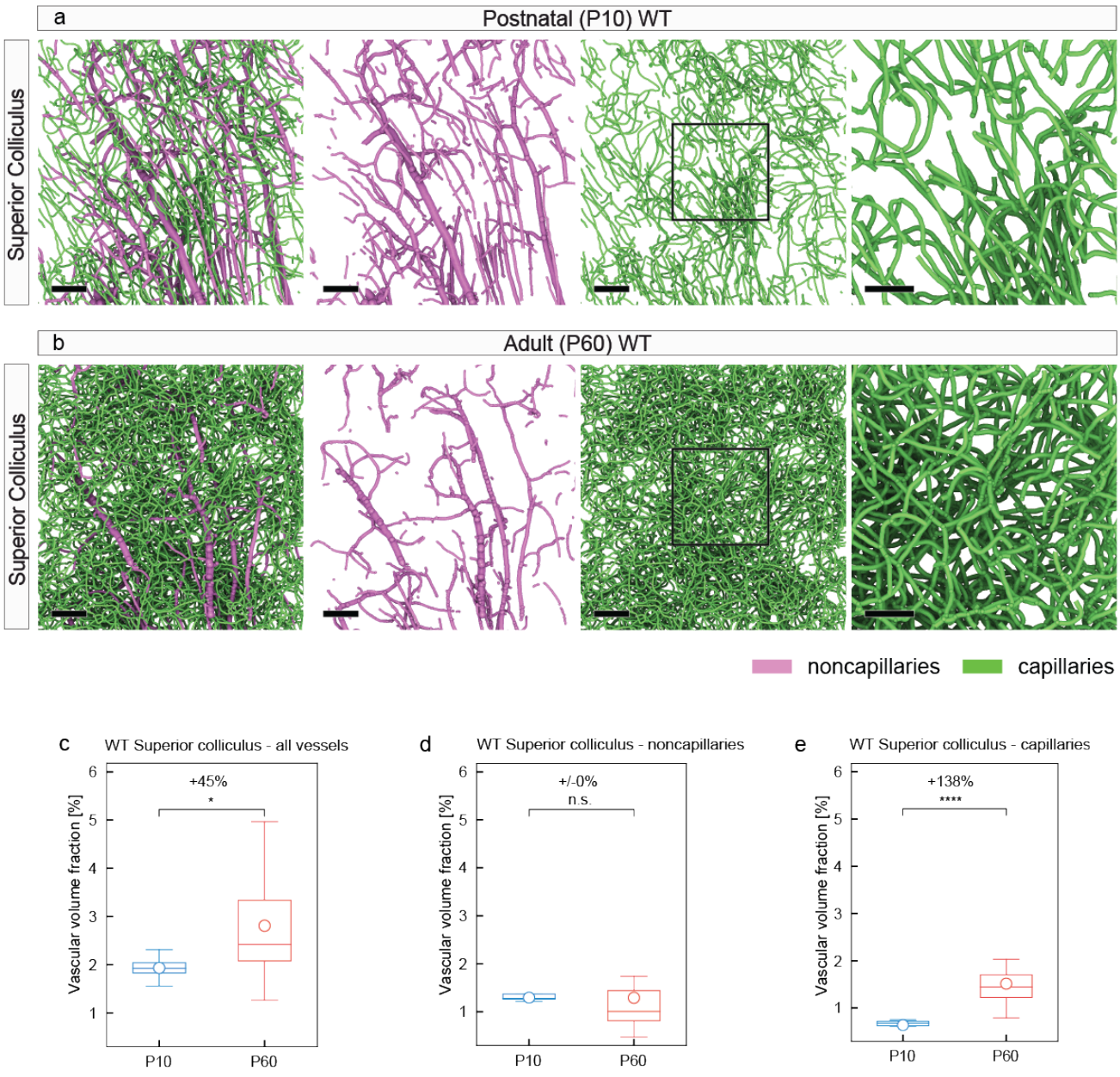

Supplementary Figure 4 Local vascular network topology – Increased vascular volume fraction of the adult (P60) WT versus postnatal (P10) WT superior colliculi mainly found at the capillary level

a,**b** Three-dimensional computational reconstruction of µCT scans of vascular networks in the superior colliculus of a P60 WT sample highlighting a vessel tree with noncapillaries in magenta and capillaries in green. **c-e** Quantification of the 3D vascular volume fraction for all vessels (**c**), noncapillaries (**d**), and capillaries (**e**) in P10 WT and P60 WT calculated by local topology analysis. The significant increase of the

vascular volume fraction for all vessels in the P60 WT animals (**c**) was mainly due to a significant increase at the level of capillaries (**e**) (n = 4-6 for P10 WT; n = 8-12 for P60 WT animals were used; and in average three ROIs per animal and brain region were used). All data are shown as mean distributions where the open dot represents the mean. Boxplots indicate the 25% to 75% quartiles of the data. The shaded blue and red areas indicate the SD. *$P < 0.05$, **$P < 0.01$, ***$P < 0.001$. Scale bars: 100 µm (**a**,**b**, overviews); 50 µm (**a**,**b**, zooms).

Supplementary Figure 5

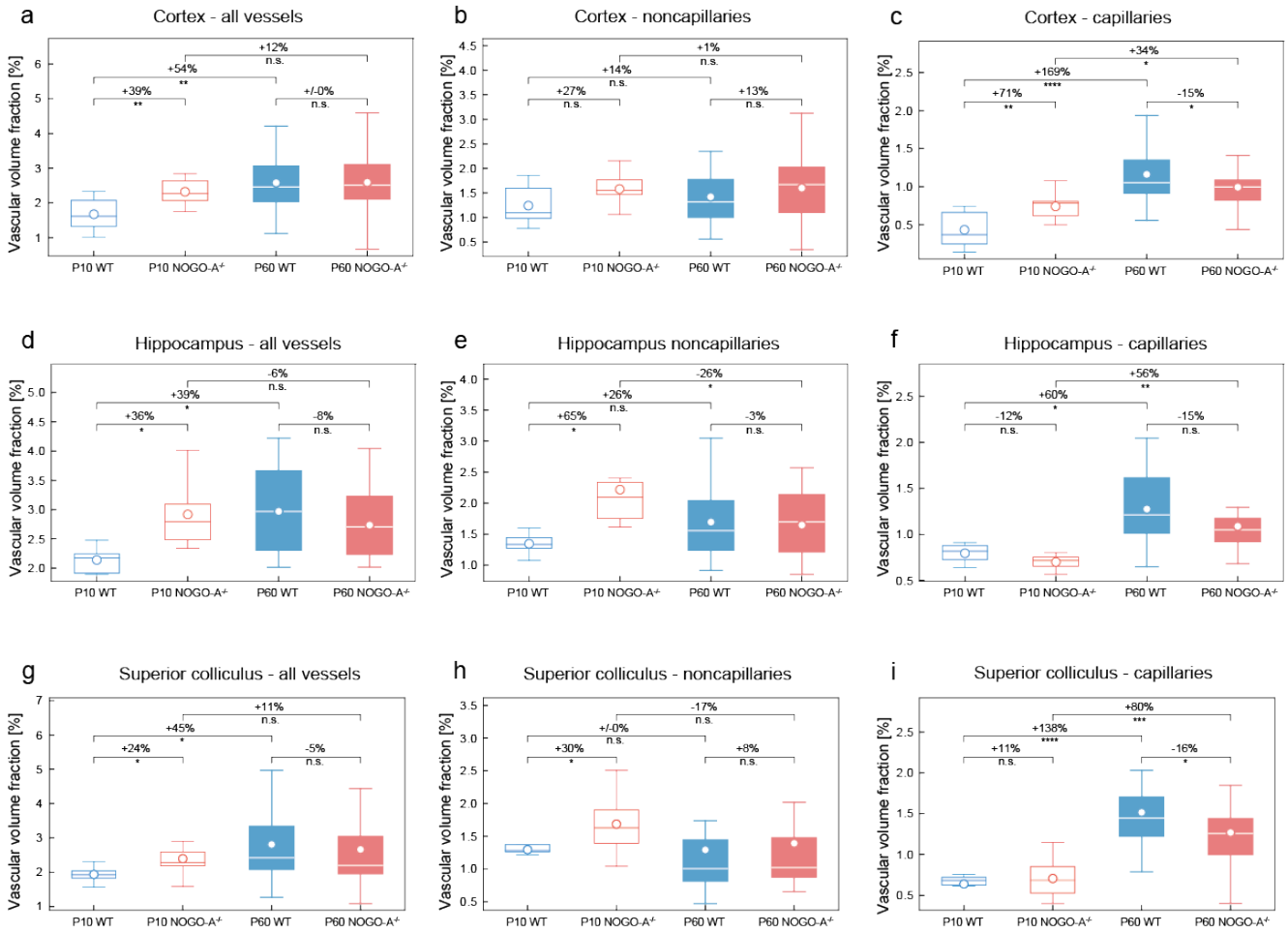

Supplementary Figure 5 Overview of the effects of physiological ageing and of genetic deletion of Nogo-A on the vascular volume fraction in various regions of the adult (P60) and postnatal (P10) mouse brain

a-i Quantification of the 3D vascular volume fraction in cortex (**a-c**), hippocampus (**d-f**), and superior colliculus (**g-i**), by computational analysis using global morphometry. The vascular volume fraction in all these brain structures was significantly higher in the Nogo-A deficient animals than that in the WT control animals. This same increase can be observed in the P60 WT group, when compared to the P10 WT animals, and is most pronounced at the level of capillaries (**c**,**f**,**i**) (n = 4-6 for P10 WT; n = 8-12 for P60 WT; n = 3-5

for P10 Nogo-A$^{-/-}$; n = 8-11 for P60 Nogo-A$^{-/-}$ animals; and in average three ROIs per animal and brain region were used). *$P < 0.05$, **$P < 0.01$, ***$P < 0.001$.

Supplementary Figure 6

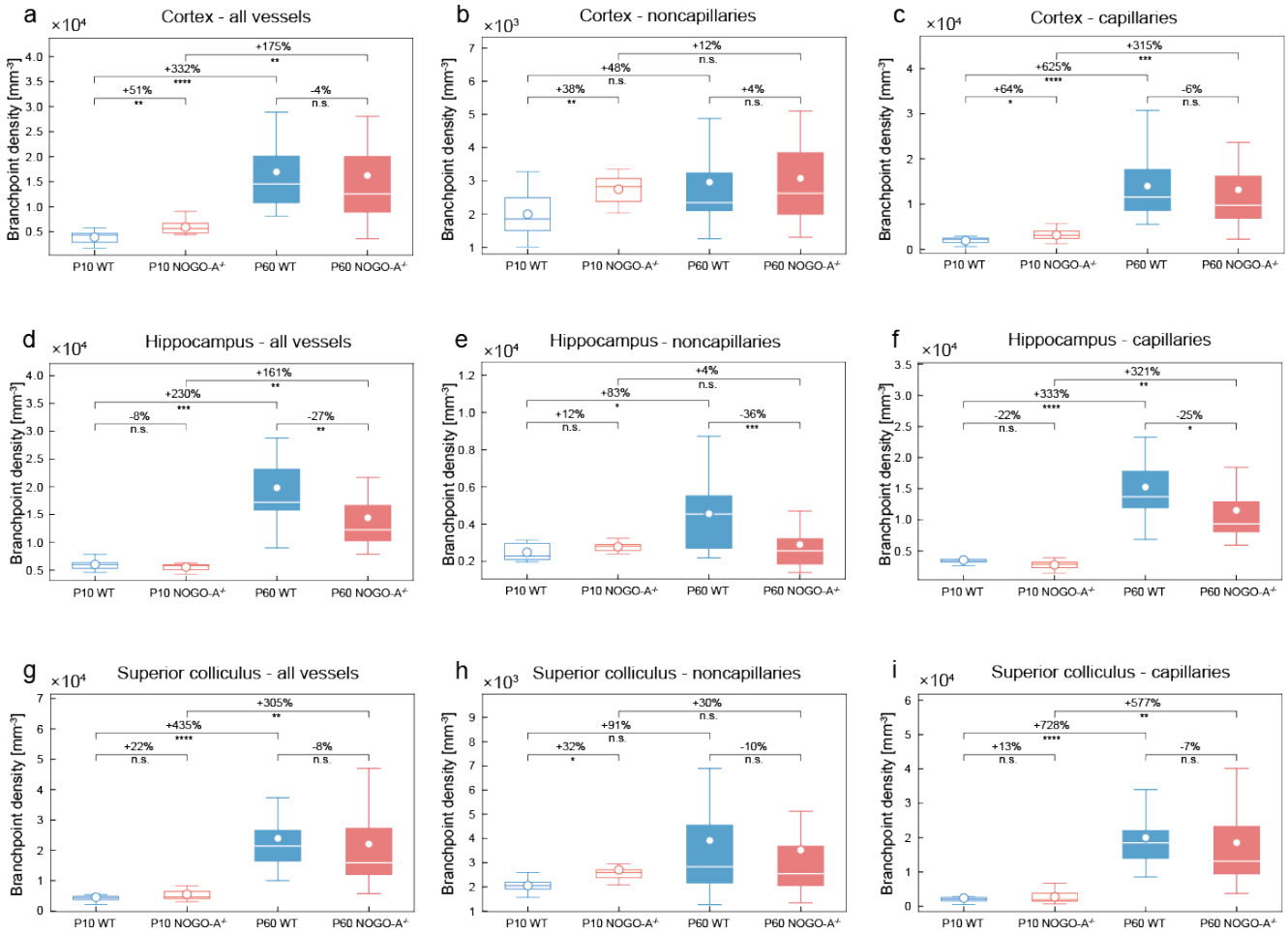

Supplementary Figure 6 Overview of the effects of physiological ageing and of genetic deletion of Nogo-A on the branch point density in various regions of the adult (P60) and postnatal (P10) mouse brain

a-i Quantification of the branch point density in cortex (**a-c**), hippocampus (**d-f**), and superior colliculus (**g-i**), by local topology analysis. The branch point density in all these brain structures was significantly higher in the Nogo-A deficient animals than that in the WT control animals. This same increase can be observed in the P60 WT group, when compared to the P10 WT animals, and is most pronounced at the level of capillaries (**c**,**f**,**i**) (n = 4-6 for P10 WT; n = 8-12 for P60 WT; n = 3-5 for P10 Nogo-A$^{-/-}$; n = 8-11 for P60 Nogo-A$^{-/-}$ animals; and in average three ROIs per animal and brain region were used). *$P < 0.05$, **$P < 0.01$, ***$P < 0.001$.

Supplementary Figure 7

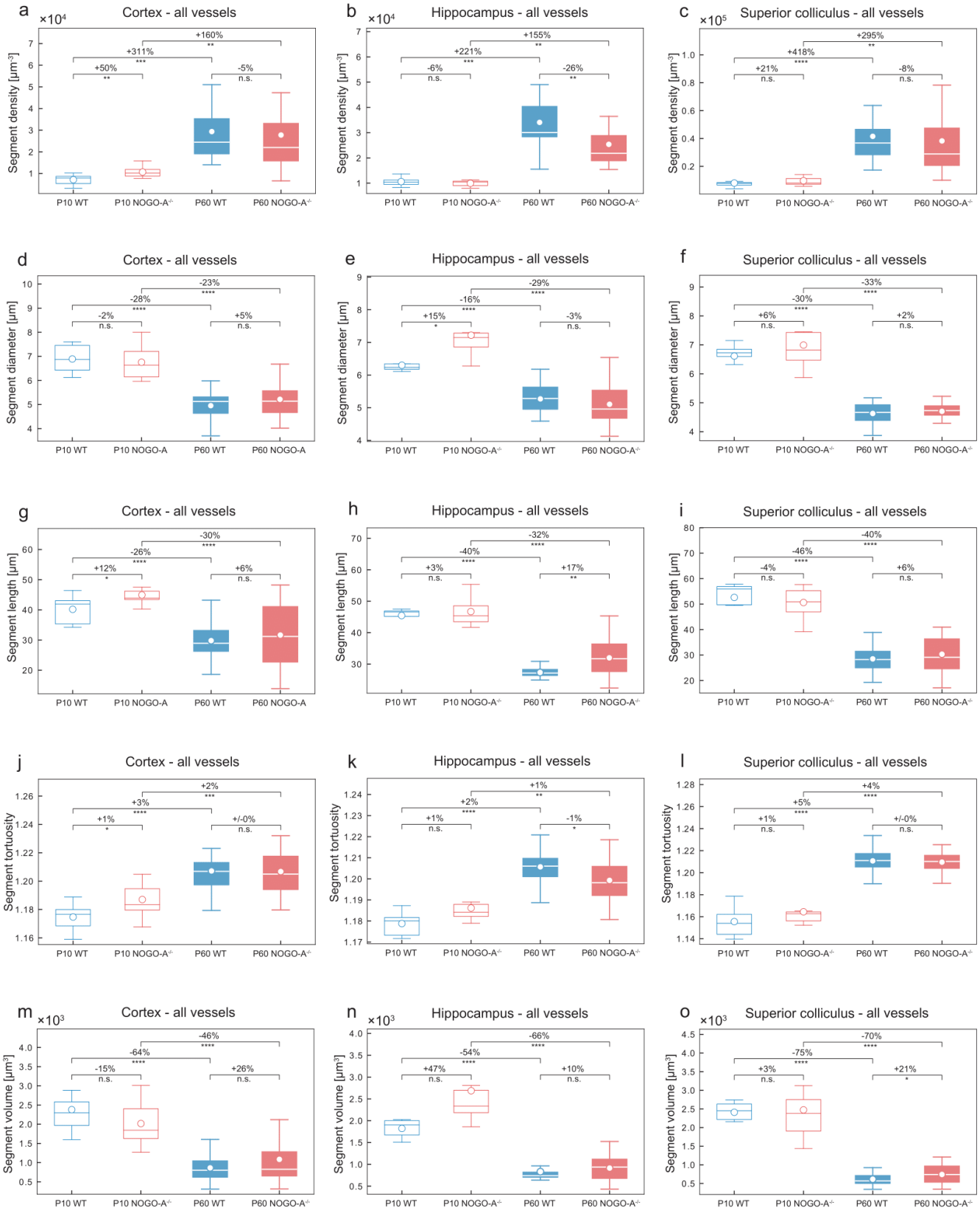

Supplementary Figure 7 Overview of the effects of physiological ageing and of genetic deletion of Nogo-A on the segment density, diameter, length, tortuosity and volume in various regions of the adult (P60) and postnatal (P10) mouse brain

a-o Quantification of segment density, diameter, length, tortuosity and volume in the cortex (**a**,**d**,**g**,**j**,**m**), hippocampus (**b**,**e**,**h**,**k**,**n**), and superior colliculus (**c**,**f**,**i**,**l**,**o**), by local topology analysis. The segment density and tortuosity in all these brain structures was significantly higher in the Nogo-A deficient animals than that in the WT control animals. This same increase can be observed in the P60 WT group, when compared to the P10 WT animals, and is most pronounced at the level of capillaries (**c**,**l**). The parameters segment diameter, length, and volume are significantly decreased in the Nogo-A deficient animals as compared to the WT control animals. Here, also this same increase, predominantly at the capillary level (**f**,**i**,**l**) can be observed in the P60 WT group, when compared to the P10 WT animals (n = 4-6 for P10 WT; n = 8-12 for P60 WT; n = 3-5 for P10 Nogo-$A^{-/-}$; n = 8-11 for P60 Nogo-$A^{-/-}$ animals; and in average three ROIs per animal and brain region were used). $*P < 0.05$, $**P < 0.01$, $***P < 0.001$.

Supplementary Figure 8

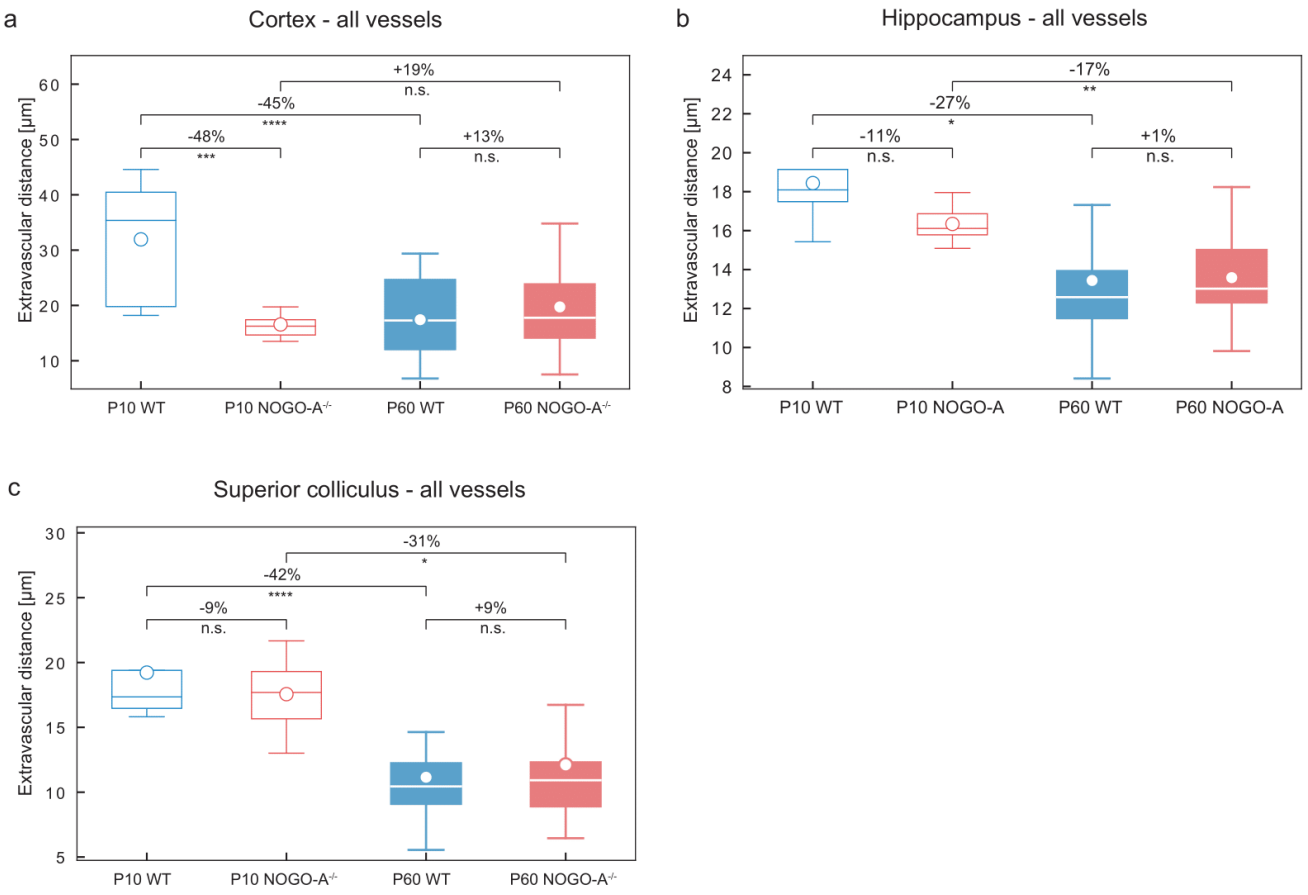

Supplementary Figure 8 Overview of the effects of physiological ageing and of genetic deletion of Nogo-A on the extravascular distance in various regions of the adult (P60) and postnatal (P10) mouse brain

a-c Quantification of the extravascular distance in P10 and P60 in the three brain regions calculated by global morphometry analysis. The extravascular distance in the cortices (**a**), hippocampi (**b**) and superior colliculi (**c**) was lower in the P10 Nogo-A deficient animals than that in the WT control animals, whereas this effect was less obvious in the P60 Nogo-A versus WT (n = 4-6 for P10 WT; n = 8-12 for P60 WT; n = 3-5 for P10 Nogo-$A^{-/-}$; n = 8-11 for P60 Nogo-$A^{-/-}$ animals; and in average three ROIs per animal and brain region were used). All data are shown as mean distributions where the open dot represents the mean. Boxplots indicate the 25% to 75% quartiles of the data. The shaded blue and red areas indicate the SD. *$P < 0.05$, **$P < 0.01$, ***$P < 0.001$.

Supplementary Figure 9

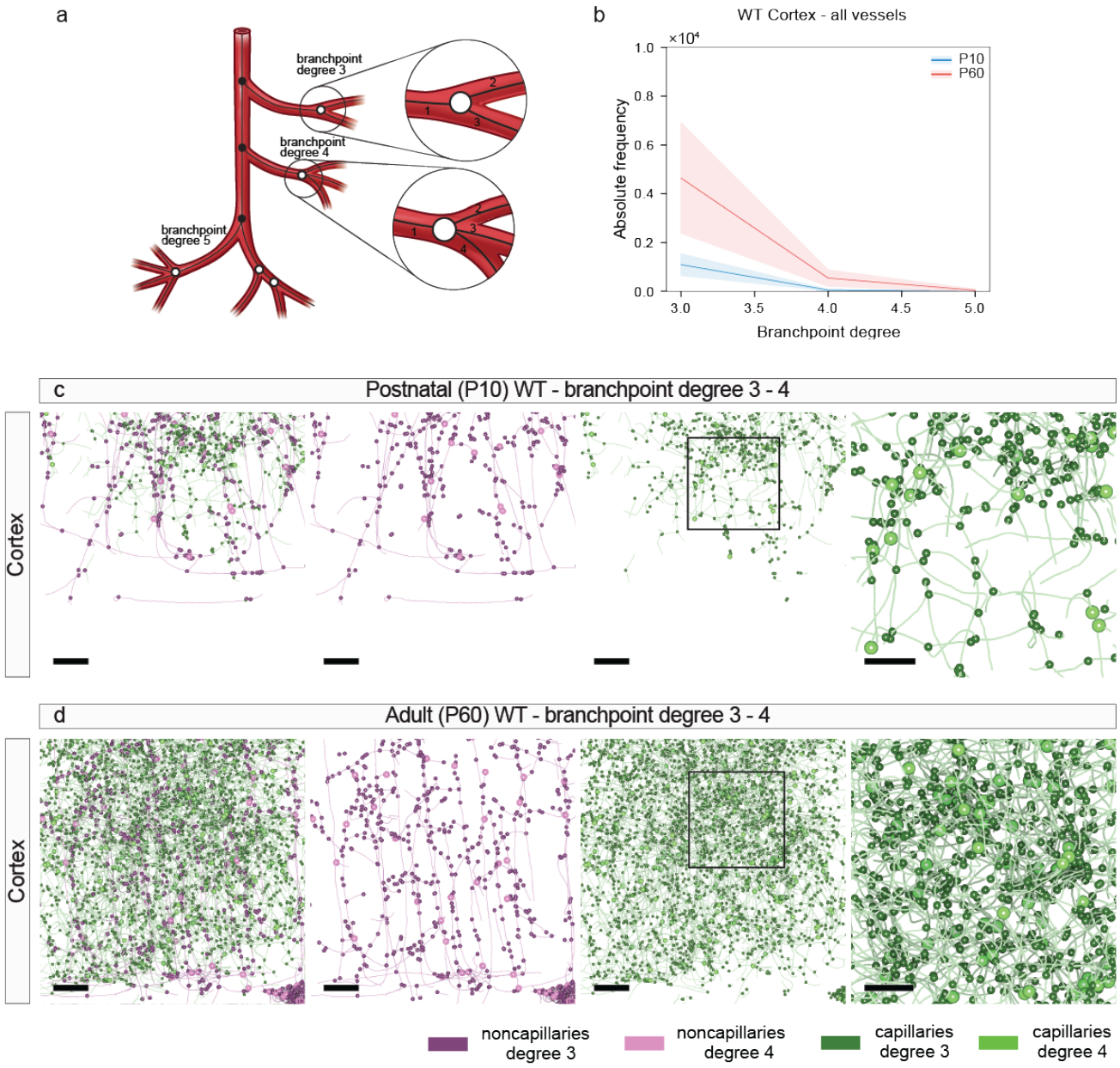

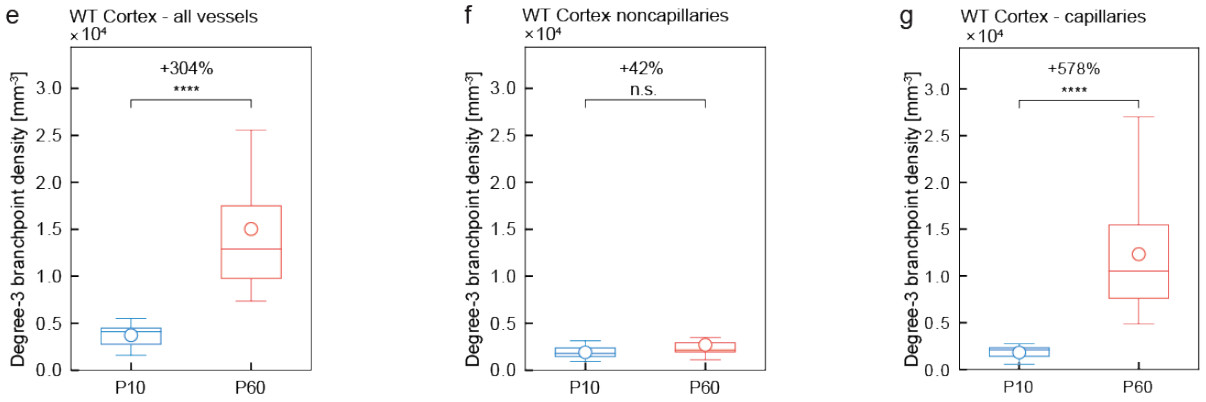

Supplementary Figure 9 continued

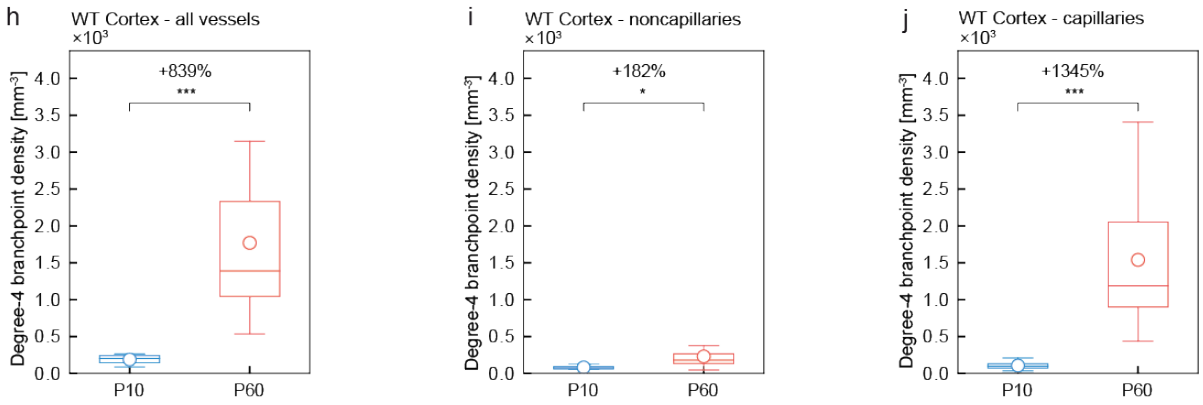

Supplementary Figure 9 Local vascular network topology – visualization and quantification of vascular branch point diameter, vascular branch point density and branch point degree in the cortex of the adult (P60) WT versus the postnatal (P10) WT mouse brain

The vascular branch point diameter and vascular branch point density are significantly increased in the P60 as compared to the P10 mouse brain cortex. **a** Scheme depicting the definition of degree 3 and 4 vascular branch point (see Figure 8b for details). **b** Histogram showing the distribution of branch point degree in P10 WT and P60 WT animals. P60 WT animals show an increased branch point degree as compared to P10 WT mice mainly at the capillary level. Of note, nearly all branch points had a degree of 3. Branch point degrees of four or even higher accounted together for far less than 1% of all branch points (bin width = 1; number of bins = 3). **c**,**d** Computational 3D reconstructions of µCT images of cortical vascular networks of P10 WT and P60 WT mice with visualizations of the vessel branch points displayed as dots, separately for noncapillaries (magenta) and capillaries (green) and for branch point degree 3 and 4 where branch points with degree 4 are enlarged and brighter than branch points with degree 3 (also see legend below **d**). The higher density of branch points in the P60 WT cortices especially at the capillary level (green) is obvious, a slight increase of branch point density can be observed at the noncapillary level (magenta). Furthermore, an increase in the branch points with degree 4 can be observed in the P60 WT (**d**) as compared to the P10 WT

(**c**) reconstructions. The boxed areas are enlarged at right (**c**,**d**). Quantitative analysis of the branch point degree-3 density for all vessels (**e**), noncapillaries (**f**), and capillaries (**g**) in P10 WT and P60 WT cortices by local morphometry analysis shows that the significant increase in density of branch points with degree-3 for all vessels in P60 WT animals (**e**) was mainly due to a significant increase at the level of capillaries (**g**) and in part due to a significant increase at the level of noncapillaries (**f**). **h-j** The same quantitative analysis for branch point degree-4 (**h-j**) shows that the significant increase of the branch points with degree-4 for all vessels in P60 WT animals (**h**) was mainly due to a highly significant and very large increase at the level of capillaries (**j**) and in part due to a significant increase at the level of noncapillaries (**i**).

In average, n = 3-12 animals were used for the cortices data; and in average three ROIs per animal were used). All data are shown as mean distributions where the open dot represents the mean. Boxplots indicate the 25% to 75% quartiles of the data. The shaded blue and red areas indicate the SD. $*P < 0.05$, $**P < 0.01$, $***P < 0.001$. Scale bars: 100 μm (**c**,**d**, overviews); 50 μm (**c**,**d**, zooms).

Supplementary Figure 10

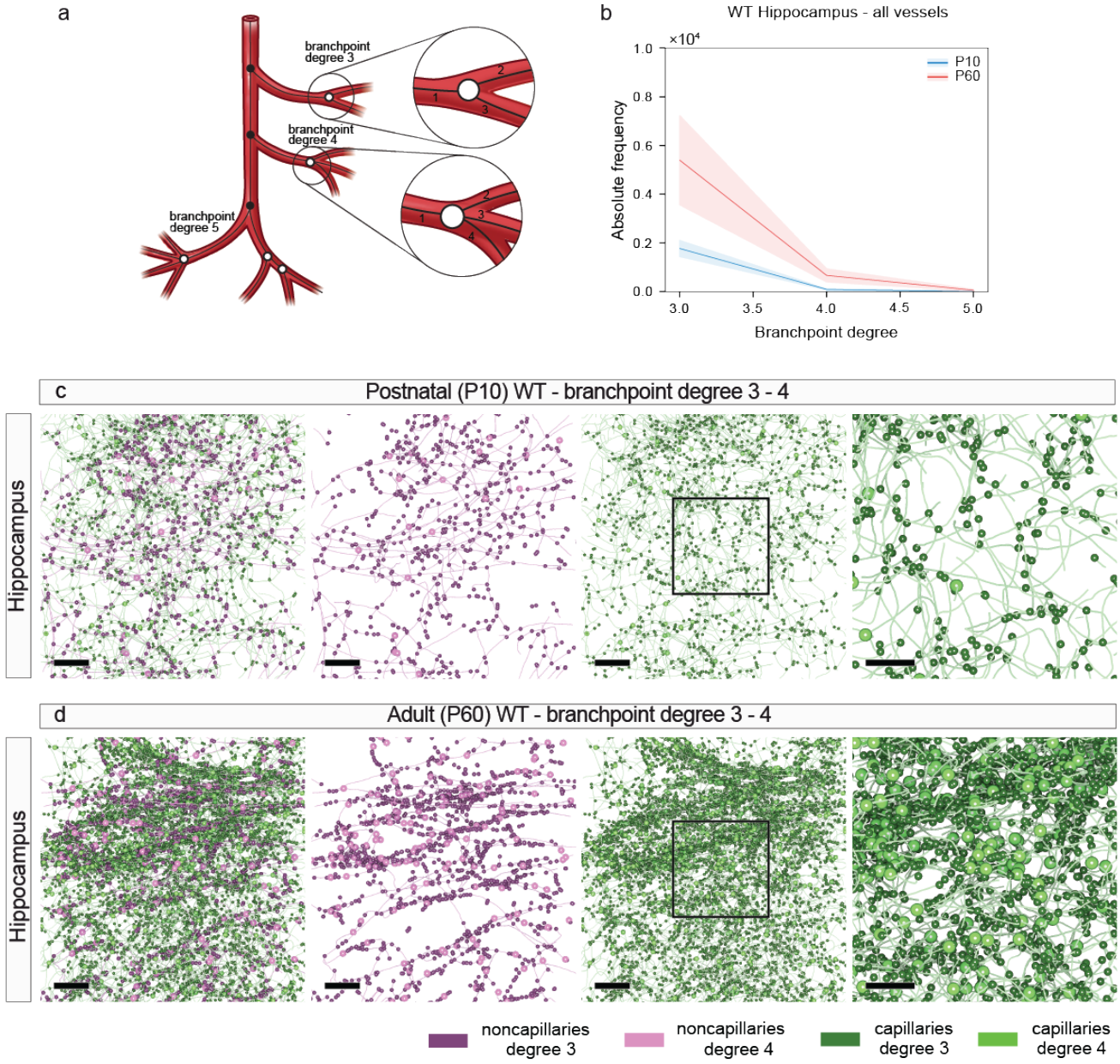

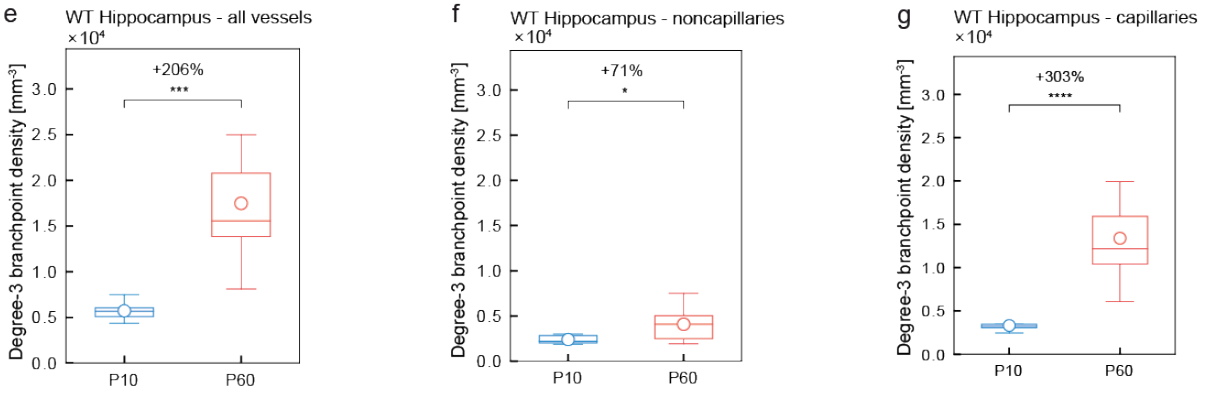

Supplementary Figure 10 continued

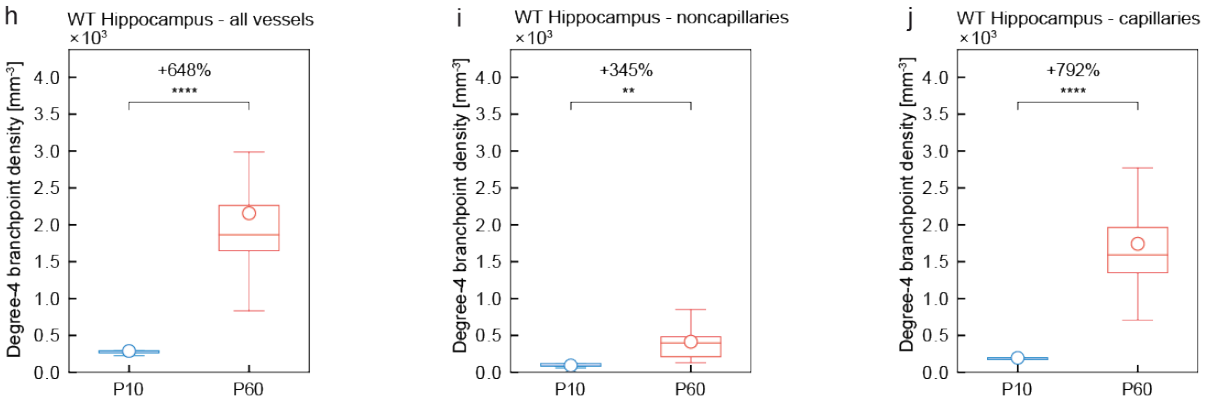

Supplementary Figure 10 Local vascular network topology – visualization and quantification of vascular branch point diameter, vascular branch point density and branch point degree in the hippocampus in the adult (P60) WT versus the postnatal (P10) mouse brain

The vascular branch point diameter and vascular branch point density are significantly increased in the P60 as compared to P10 mouse brain hippocampus. **a** Scheme depicting the definition of vascular branch points (see Figure 8b for details). **b** Histogram showing the distribution of branch point diameter in P10 WT and P60 WT animals. P60 WT animals show an increased branch point degree as compared to P10 WT mice mainly at the capillary level. Of note, nearly all branch points had a degree of 3. Branch point degrees of four or even higher accounted together for far less than 1% of all branch points (bin width = 1; number of bins = 3). **c**,**d** Computational 3D reconstructions of µCT images of vascular networks of P10 WT and P60 WT mice with visualizations of the vessel branch points displayed as dots, separately for noncapillaries (magenta) and capillaries (green) and for branch point degree 3 and 4 where branch points with degree 4 are enlarged and brighter than branch points with degree 3 (see legend). The higher density of branch points in the P60 WT hippocampi especially at the capillary level (green) is obvious, a slight increase of branch point density can be observed at the noncapillary level (magenta). The boxed areas are enlarged at right (**c**,**d**). Quantitative analysis of the branch point degree-3 density for all vessels (**e**), noncapillaries (**f**), and capillaries (**g**) in P10

WT and P60 WT hippocampi by local morphometry analysis shows that the significant increase in density of branch points with degree-3 for all vessels in the P60 WT animals (**e**) was mainly due to a significant increase at the level of capillaries (**g**) and in part due to a significant increase at the level of noncapillaries (**f**). **h-j** The same quantitative analysis for branch point degree-4 (**h-j**) shows that the significant increase of the branch points with degree-4 for all vessels in the P60 WT animals (**h**) was mainly due to a highly significant and very large increase at the level of capillaries (**j**) and in part due to a significant increase at the level of noncapillaries (**i**).

In average, n = 2-7 animals were used for the hippocampi; and in average three ROIs per animal and brain region were used. All data are shown as mean distributions where the open dot represents the mean. Boxplots indicate the 25% to 75% quartiles of the data. The shaded blue and red areas indicate the SD. **P* < 0.05, ***P* < 0.01, ****P* < 0.001. Scale bars: 100 µm (**c**,**d**, overviews); 50 µm (**c**,**d**, zooms).

Supplementary Figure 11

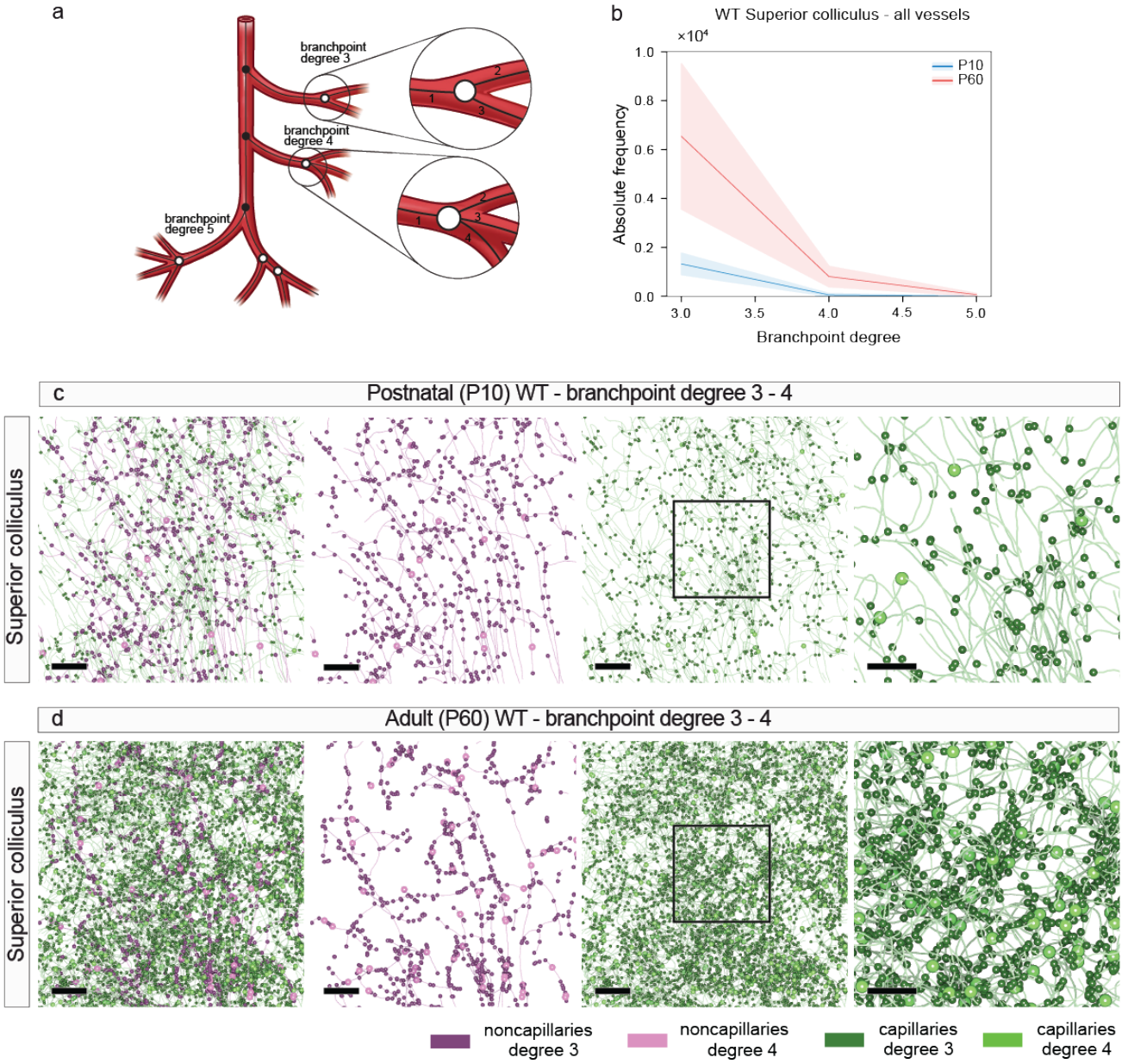

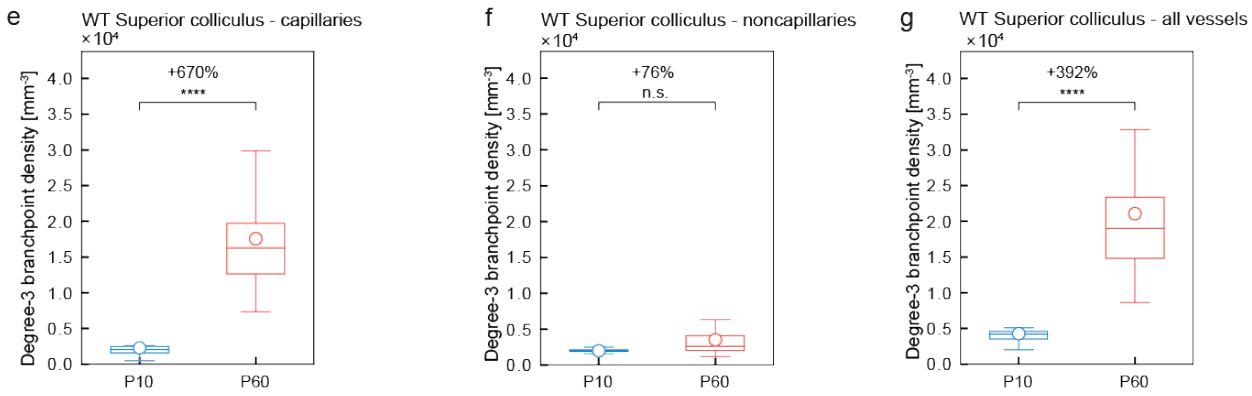

Supplementary Figure 11 continued

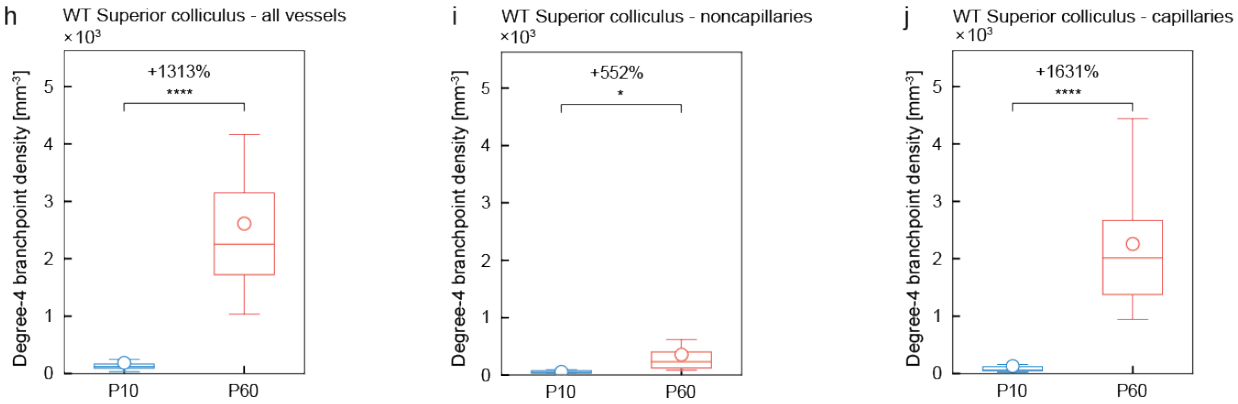

Supplementary Figure 11 Local vascular network topology – visualization and quantification of vascular branch point diameter, vascular branch point density and branch point degree in the superior colliculus of the adult (P60) WT versus the postnatal (P10) WT mouse brain.

The vascular branch point diameter and vascular branch point density are significantly increased in the P60 as compared to the P10 mouse brain superior colliculi **a** Scheme depicting the definition of vascular branch points (see Figure 8b for details). **b** Histogram showing the distribution of branch point diameter in P10 WT and P60 WT animals. P60 WT animals show an increased branch point density as compared to P10 WT mice mainly at the capillary level. Of note, nearly all branch points had a degree of 3. Branch point degrees of four or even higher accounted together for far less than 1% of all branch points (bin width = 1; number of bins = 3). **c**,**d** Computational 3D reconstructions of µCT images of vascular networks of P10 WT and P60 WT mice with visualizations of the vessel branch points displayed as dots, separately for noncapillaries (magenta) and capillaries (green) and for branch point degree 3 and 4 where branch points with degree 4 are enlarged and brighter than branch points with degree 3 (see legend). The higher density of branch points in the P60 WT superior colliculi especially at the capillary level (green) is obvious, a slight increase of branch point density can be observed at the noncapillary level (magenta). The boxed areas are enlarged at right. Quantitative analysis of the branch point density for all vessels (**e**), noncapillaries (**f**), and capillaries (**g**) in P10 WT and

P60 WT superior colliculi by local morphometry analysis. The significant increase of the branch point density for all vessels in the P60 WT animals (**e**) was mainly due to a significant increase at the level of capillaries (**g**) and in part due to a significant increase at the level of noncapillaries (**f**). **h-j** The same quantitative analysis for branch point degree-4 (**h-j**) shows that the significant increase of the branch points with degree-4 for all vessels in the P60 WT animals (**h**) was mainly due to a highly significant and very large increase at the level of capillaries (**j**) and in part due to a significant increase at the level of noncapillaries (**i**). In average, n = 2-4 animals were used for the superior colliculi; and in average three ROIs per animal and brain region were used. All data are shown as mean distributions where the open dot represents the mean. Boxplots indicate the 25% to 75% quartiles of the data. The shaded blue and red areas indicate the SD. *$P < 0.05$, **$P < 0.01$, ***$P < 0.001$. Scale bars: 100 μm (**c**,**d**, overviews); 50 μm (**c**,**d**, zooms).

Supplementary Figure 12

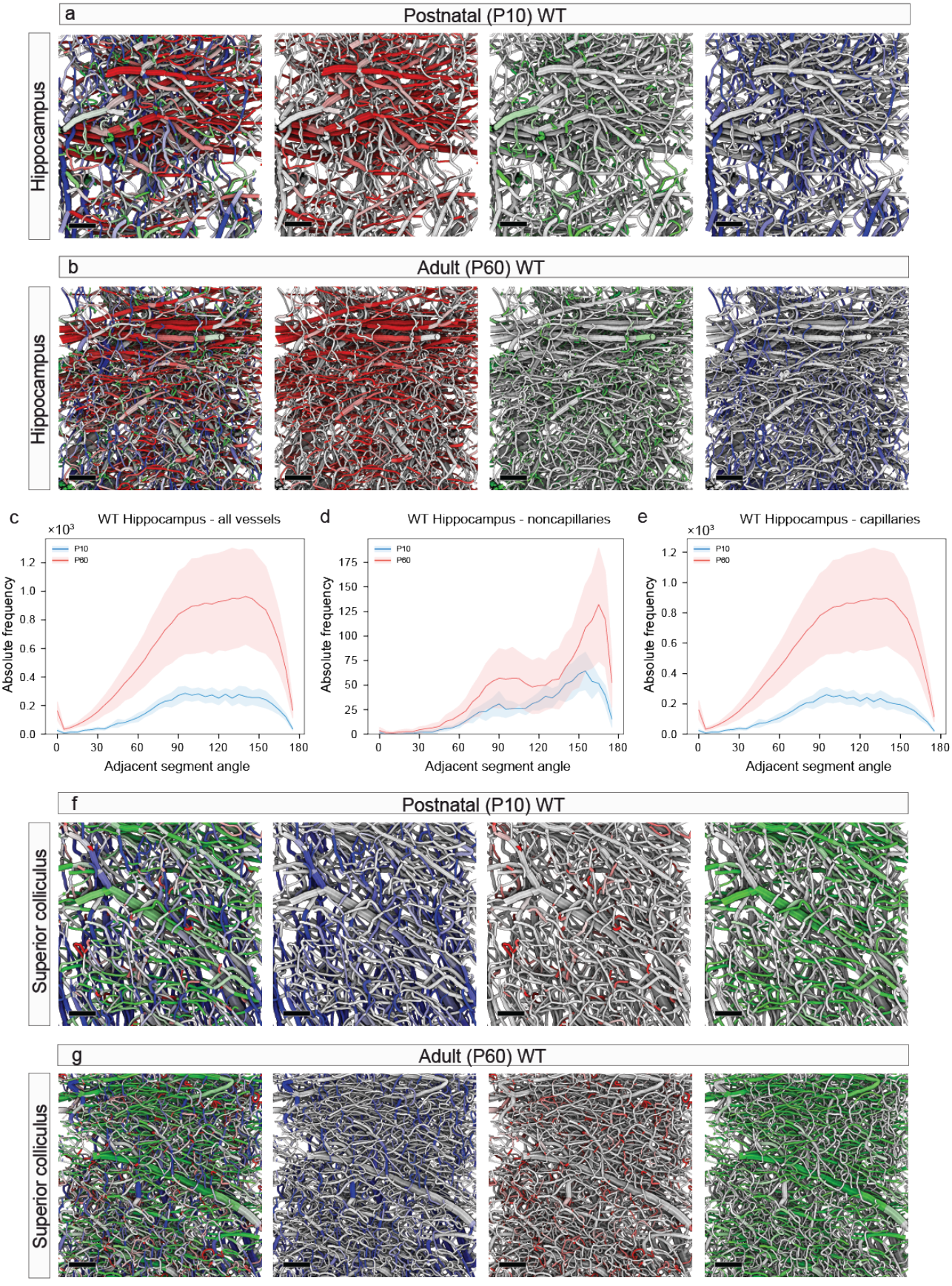

Supplementary Figure 12 continued

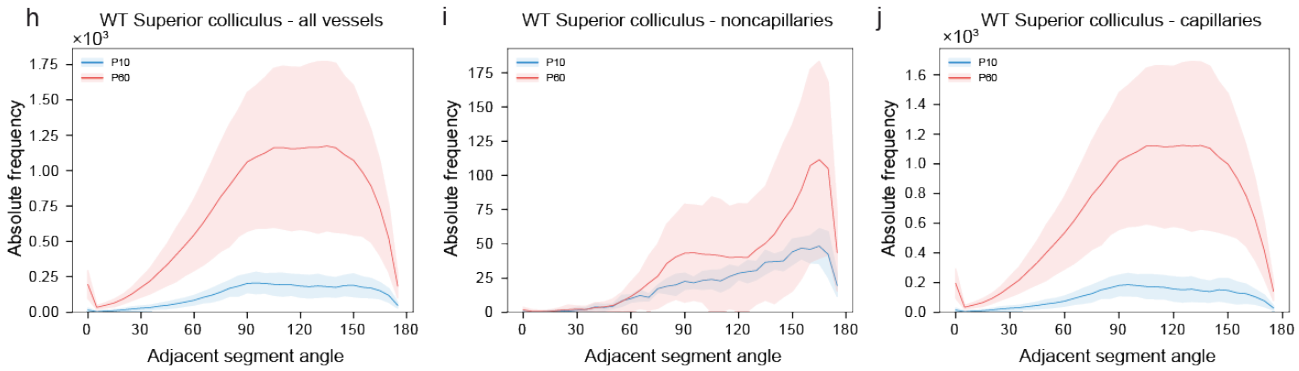

Supplementary Figure 12 Global vascular network morphology – visualization of distinct patterns of vessel directionality in the hippocampus and superior colliculus of the adult (P60) WT and postnatal (P10) WT mouse brain

Computational 3D reconstruction of µCT scans of hippocampal and superior colliculi vascular networks of P60 WT displayed with color-coded directionality obtained by attributing every vessel segment to its main direction in the x (red), y (green), and z (blue) planes within the selected ROIs (see Figure 12a for details). **a,b** Computational 3D reconstruction of µCT scans color-coded for vessel directionality depicting the P10 WT (**a**) and P60 WT (**b**) hippocampus. In the hippocampus, horizontally orientated main vessel branches in the x-axis were recognizable, most likely following the distinct curved shape of this anatomical structure. **f**,**g** In the superior colliculus, a comparable pattern of directionality as in the cortex was observed with recognizable INVP vessels radially sprouting into the brain parenchyma along the z-axis. **c-e**,**h-j** Quantitative analysis showing histograms for the distribution of the relative angles of the vascular segments emanating from a certain branch point (segment angle for adjacent vessels) in P10 and P60 animals in the hippocampus (**c-e**), and superior colliculus (**h-j**). Noncapillaries revealed two main angles of orientation, namely around 90° and at around 170° in the three brain regions examined (**d** for hippocampus, **i** for superior colliculus), and these two main angles of orientation were more pronounced at the adult P60 as compared to the developing P10 stage (**d**,**i**), and were very similar in the brain regions, suggesting a more general underlying

concept of vessel directionality/orientation. The capillaries derived at angles between around 75° and 150° at both the developing P10 and mature P60 stages in the hippocampus (**e**), and superior colliculus (**j**) (**c-e**,**h-j** bin width = 5; number of bins = 55). Scale bars: 100 μm (**a**,**b**,**f**,**g**).

Supplementary Figure 13

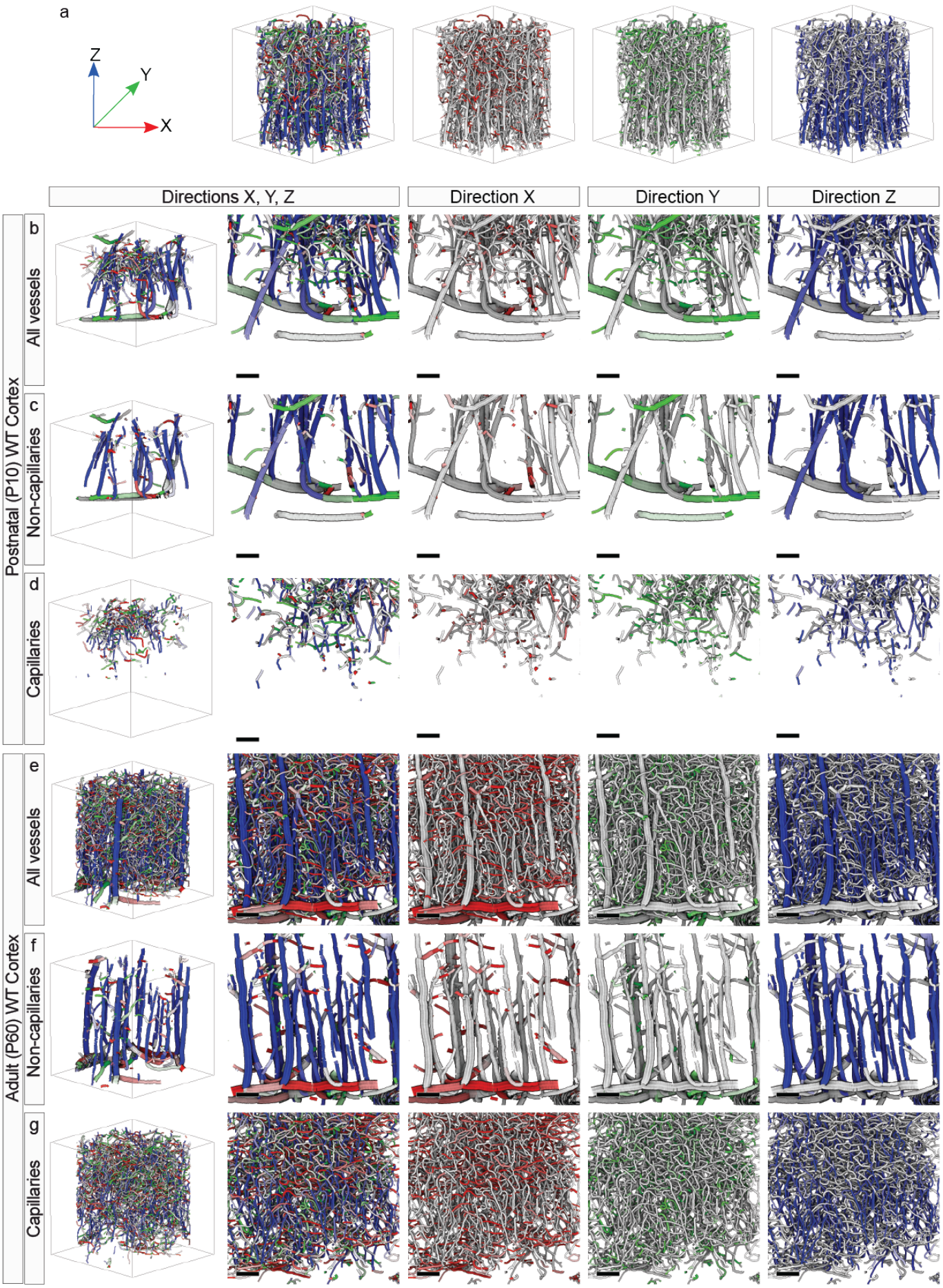

Supplementary Figure 13 Global vascular network morphology – visualization of distinct patterns of vessel directionality in the cortex of the adult (P60) WT and postnatal (P10) WT mouse brain with a division into capillaries and noncapillaries

a Computational 3D reconstruction of µCT scans of vascular networks of P60 WT displayed with color-coded directionality (see Figure 12 for details). **b-g** Computational 3D reconstruction of µCT scans color-coded for vessel directionality depicting the P10 WT (**b-d**) and P60 WT (**e-g**) cortex. A division was made between all vessels (**b**,**e**), noncapillaries (**c**,**f**), and capillaries (**d**,**g**), defined by an inner diameter of ≥ 7 µm for noncapillaries and < 7 µm for capillaries. Cortical renderings clearly showed that the superficial perineural vascular plexus (PNVP) extended in the x- and y-directions, whereas the interneural vascular plexus (INVP) exhibited a radial sprouting pattern into the brain parenchyma along the z-axis, perpendicular to the PNVP, in accordance with literature[1-3]. The distinction between noncapillaries and capillaries revealed that the PNVP and INVP were mainly composed of noncapillary vessels (**c**,**f**). Vessel sprouts emanating from the base of these main vessel branches (noncapillaries) of the INVP (and to a lesser extent of the PNVP) in the x-.y-, and z-directions were identified as capillaries. These capillaries vascularized the cortical CNS parenchyma via sprouting from noncapillaries and extended in all directions (x-,y-,z-), thereby assuring adequate microvascularization and perfusion of the brain (**d**,**g**). At the adult stage, these patterns of vessel directionality observed at the postnatal developing stage were confirmed and further strengthened. Scale bars: 100 µm (**b-g**).

Supplementary Figure 14

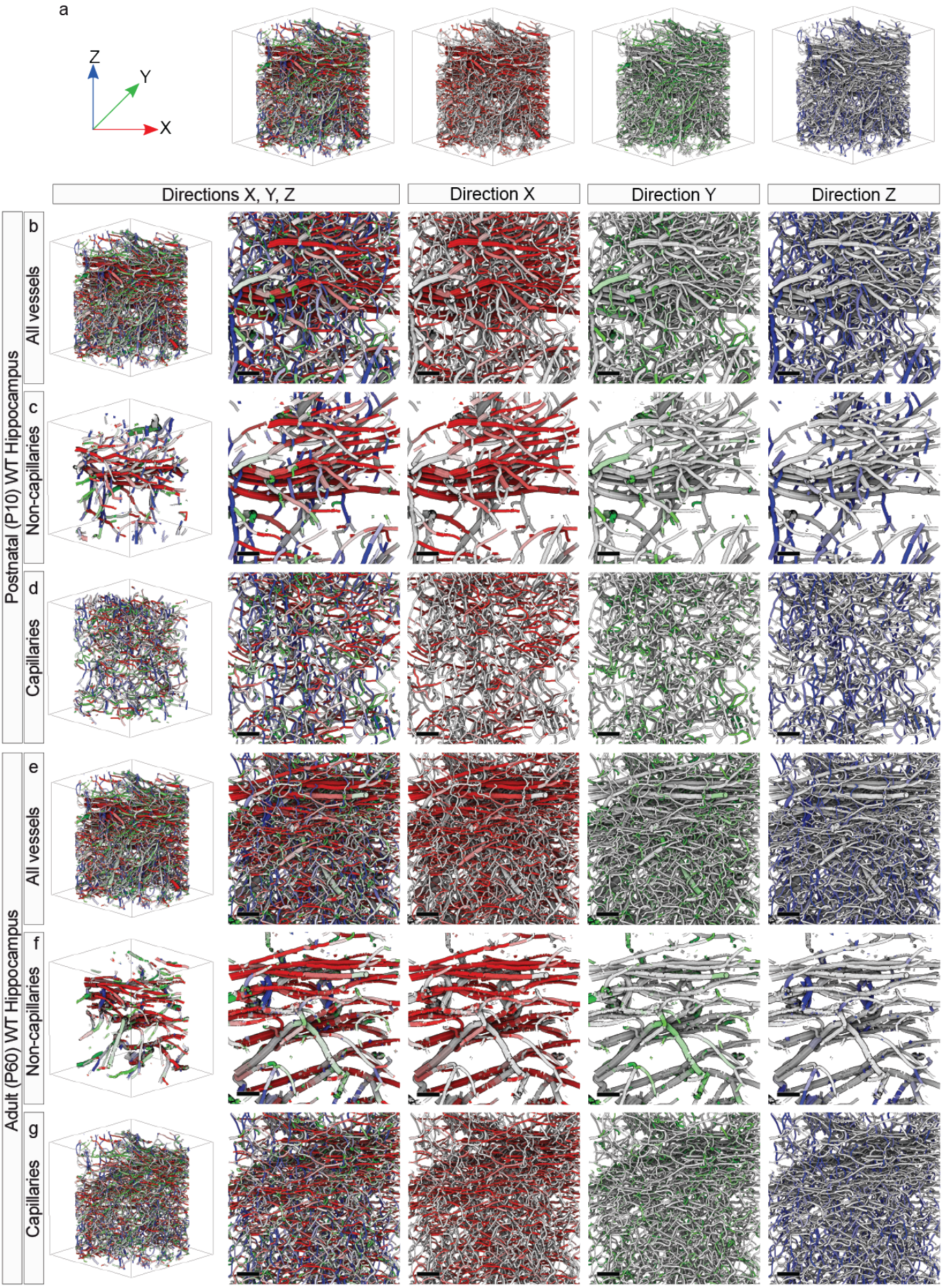

Supplementary Figure 14 Global vascular network morphology – visualization of distinct patterns of vessel directionality in the hippocampus of the adult (P60) WT and postnatal (P10) WT mouse brain with a division into capillaries and noncapillaries

a Computational 3D reconstruction of µCT scans of vascular networks of P60 WT displayed with color-coded directionality (see Figure 12 for details). **b-g** Computational 3D reconstruction of µCT scans color-coded for vessel directionality depicting the P10 WT (**b-d**) and P60 WT (**e-g**) hippocampus. A division was made between all vessels (**b**,**e**), noncapillaries (**c**,**f**), and capillaries (**d**,**g**), defined by an inner diameter of ≥ 7 µm for noncapillaries and < 7 µm for capillaries. In the hippocampus, horizontally orientated main vessel branches in the x-axis were recognizable, most likely following the distinct curved shape of this anatomical structure. Differentiation between noncapillary and capillary vessel structures (**b**,**e**) indicated that these main vessel branches were mainly composed of noncapillary vessels (**c**,**f**). Similar to what we observed in the cortex, vessel sprouts emanating from the base of these main vessel branches (noncapillaries) in the x-, y-, and z-directions were identified as capillaries (**d**,**g**). These capillaries mostly formed the smaller side branches sprouting into the four subregions of the hippocampus proper (CA1, CA2, CA3, dentate gyrus) (**d**,**g**), similar to the human hippocampal vascularization pattern[4,5]. Scale bars: 100 µm (**b-g**).

Supplementary Figure 15

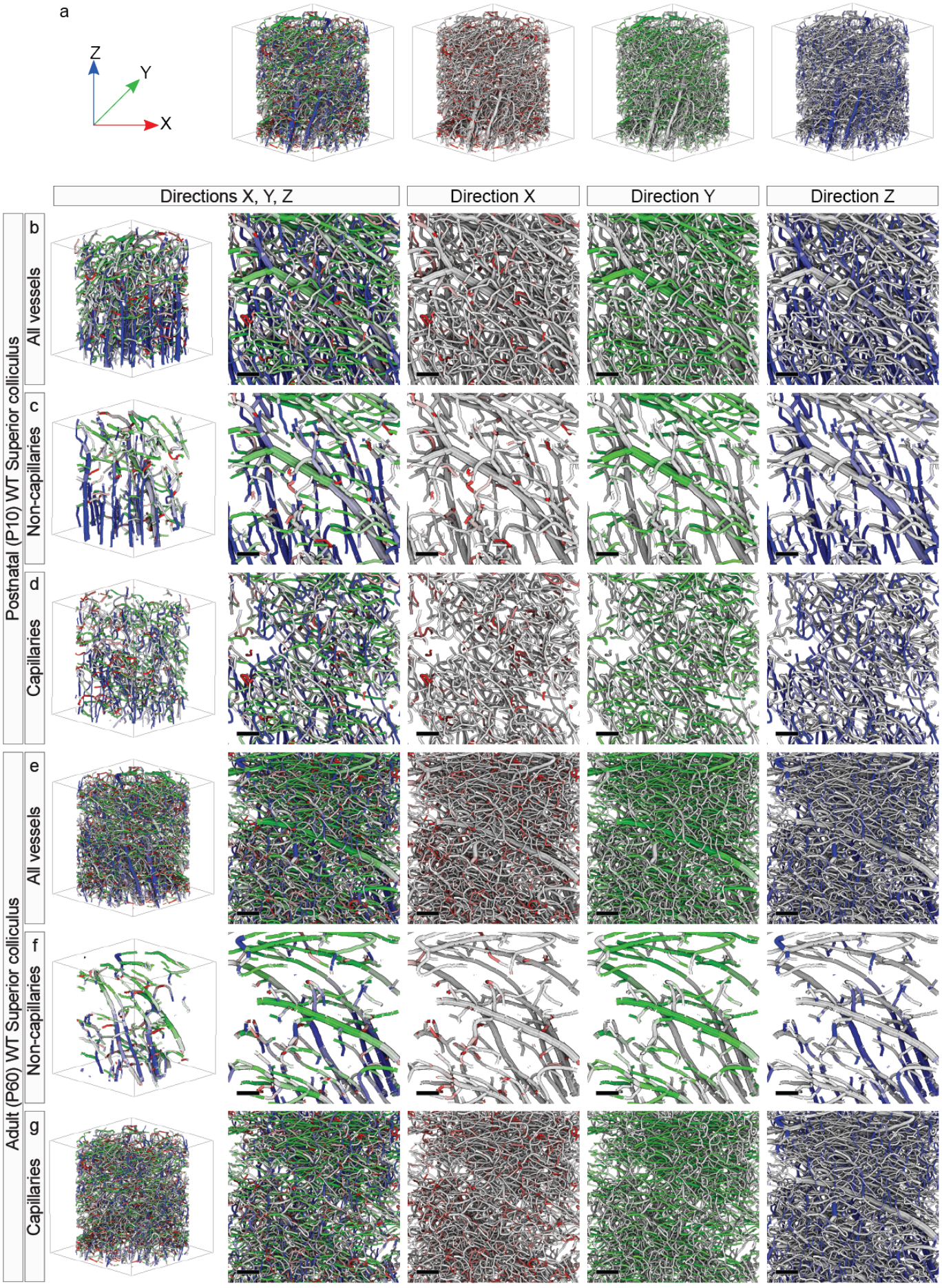

Supplementary Figure 15 Global vascular network morphology – visualization of distinct patterns of vessel directionality in the superior colliculus of the adult (P60) WT and postnatal (P10) WT mouse brain with a division into capillaries and noncapillaries

a Computational 3D reconstruction of µCT scans of vascular networks of P60 WT displayed with color-coded directionality (see Figure 12 for details). **b-g** Computational 3D reconstruction of µCT scans color-coded for vessel directionality depicting the P10 WT (**b-d**) and P60 WT (**e-g**) cortex. A division was made between all vessels (**b**,**e**), noncapillaries (**c**,**f**), and capillaries (**d**,**g**), defined by an inner diameter of ≥ 7 µm for noncapillaries and < 7 µm for capillaries. In the superior colliculus, a comparable pattern of directionality as in the cortex was observed with recognizable INVP vessels radially sprouting into the brain parenchyma along the z-axis. (**c**,**f**). Differentiation between noncapillary and capillary vessel structures (**b**,**e**) indicated that these main vessel branches were mainly composed of noncapillary vessels (**c**,**f**). Similar to what we observed in the cortex, vessel sprouts emanating from the base of these main vessel branches (noncapillaries) in the x-, y-, and z-directions were identified as capillaries (**d**,**g**). Scale bars: 100 µm (**b-g**).

Supplementary Figure 16

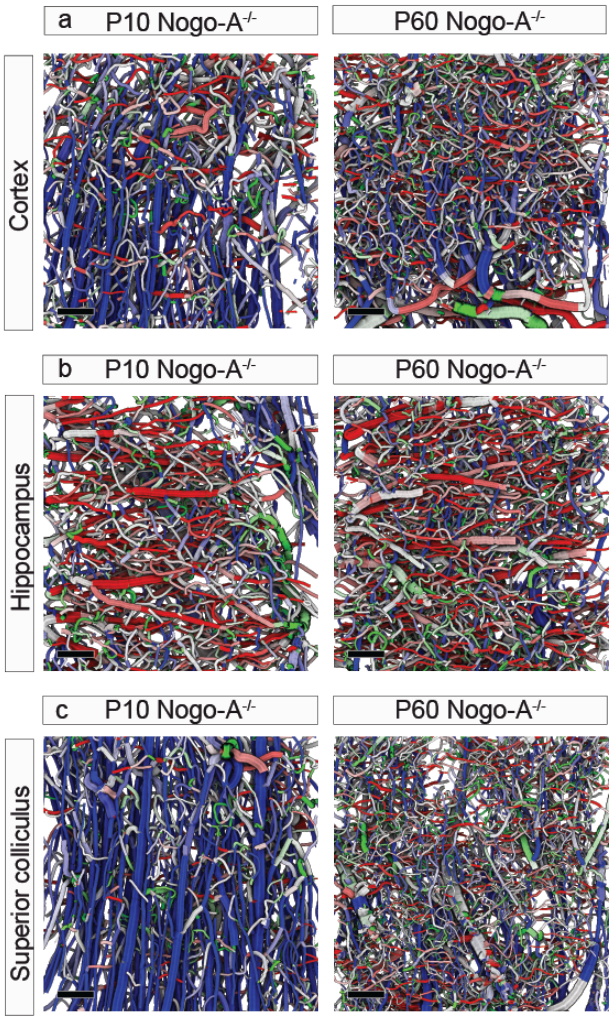

Supplementary Figure 16 Global vascular network morphology – visualization of distinct patterns of vessel directionality in various brain regions of the adult (P60) Nogo-A$^{-/-}$ and postnatal (P10) Nogo-A$^{-/-}$ mouse brain

a Computational 3D reconstruction of µCT scans color-coded for vessel directionality depicting the P10 Nogo-A$^{-/-}$ and P60 Nogo-A$^{-/-}$ cortex (see Figure 12 for details). Cortical renderings clearly show that the superficial PNVP extended in the x- and y-directions, whereas the INVP exhibited a radial sprouting pattern into the brain parenchyma along the z-axis, perpendicular to the PNVP. **b** In the hippocampus, horizontally orientated main vessel branches in the x-axis were recognizable, most likely following the distinct curved shape of this anatomical structure. **c** In the superior colliculus, a comparable pattern of directionality as in

the cortex was observed with recognizable INVP vessels radially sprouting into the brain parenchyma along the z-axis. Scale bars: 100 μm (**b-g**).

Supplementary Figure 17

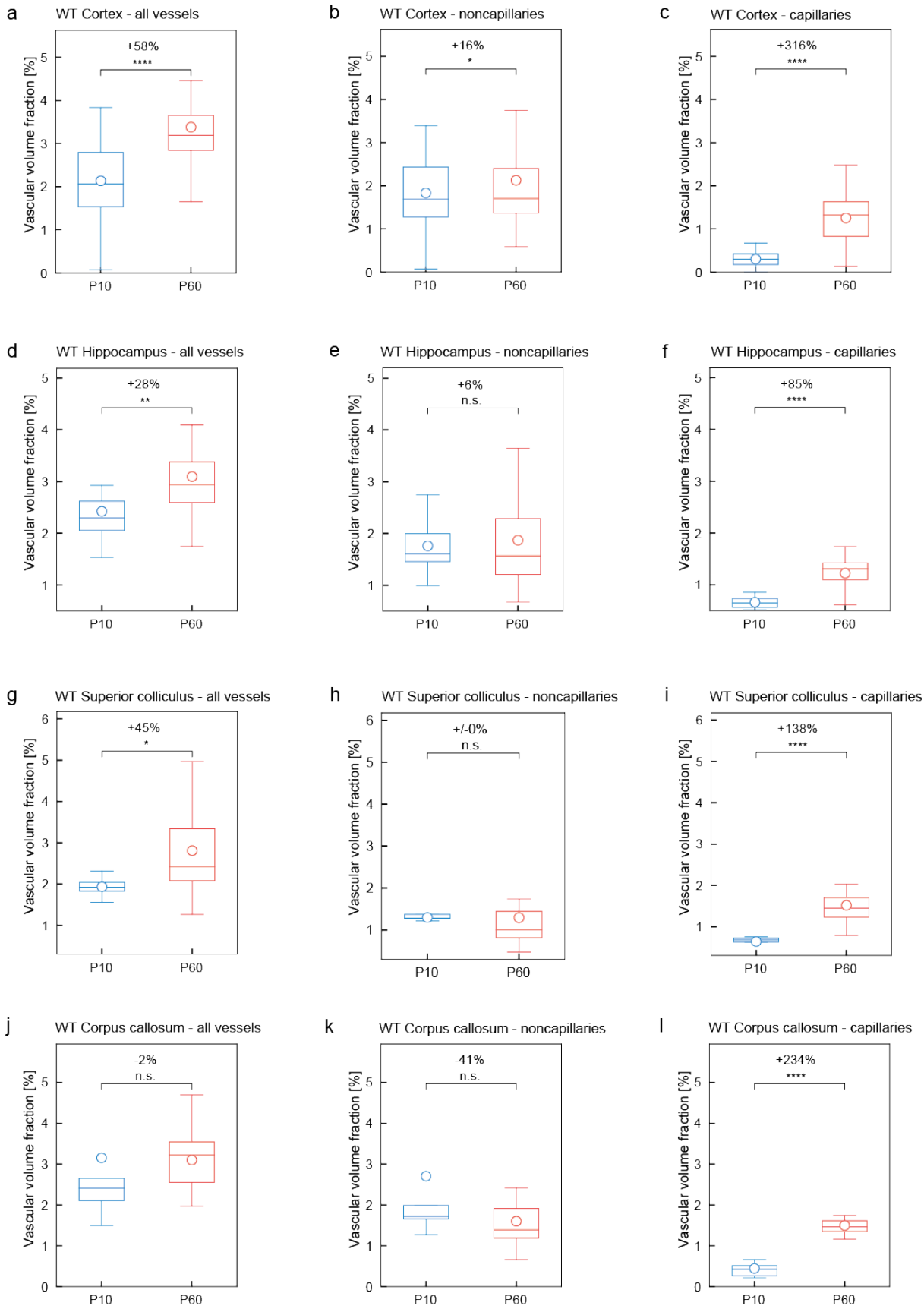

Supplementary Figure 17 continued 1/3

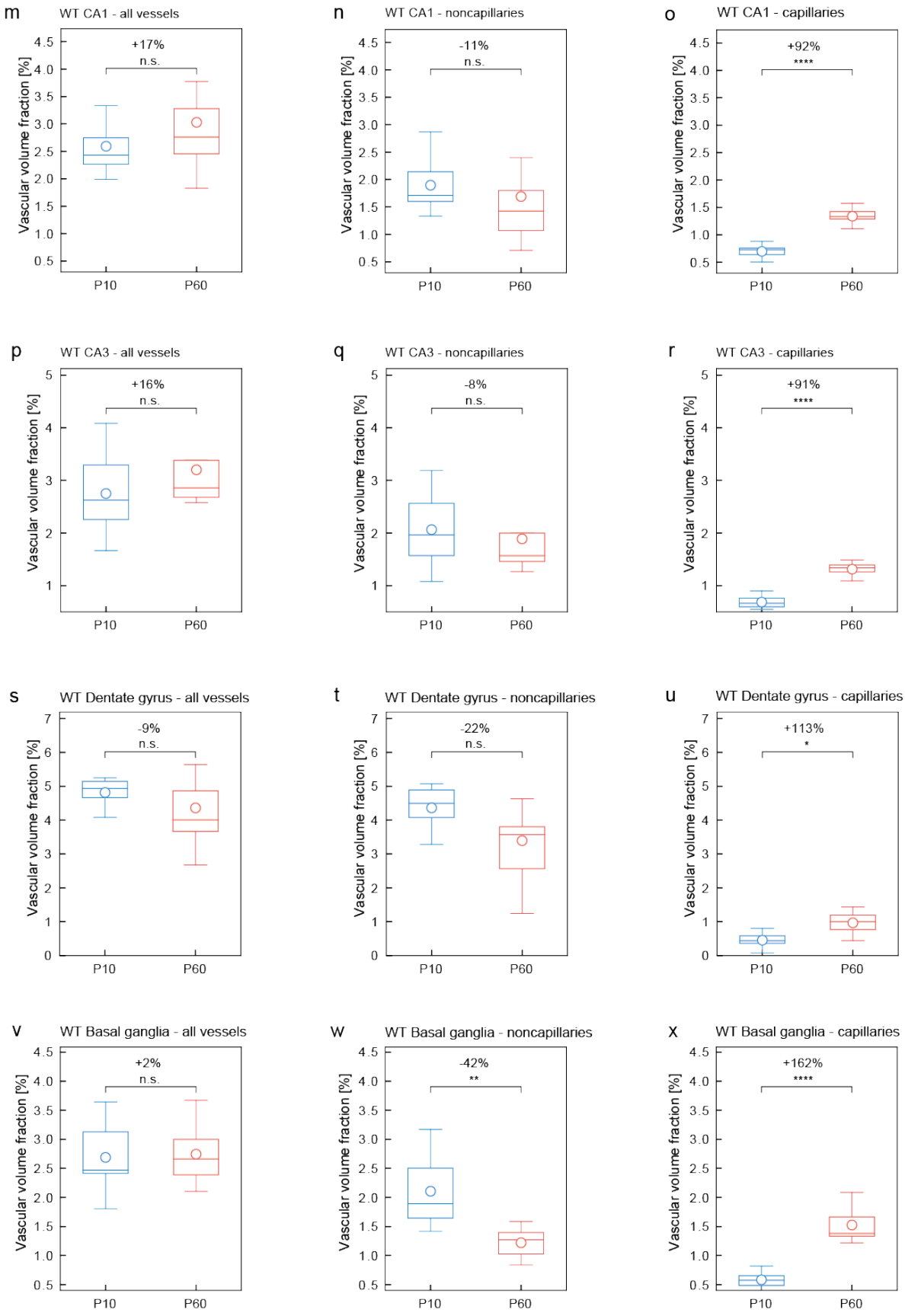

Supplementary Figure 17 continued 2/3

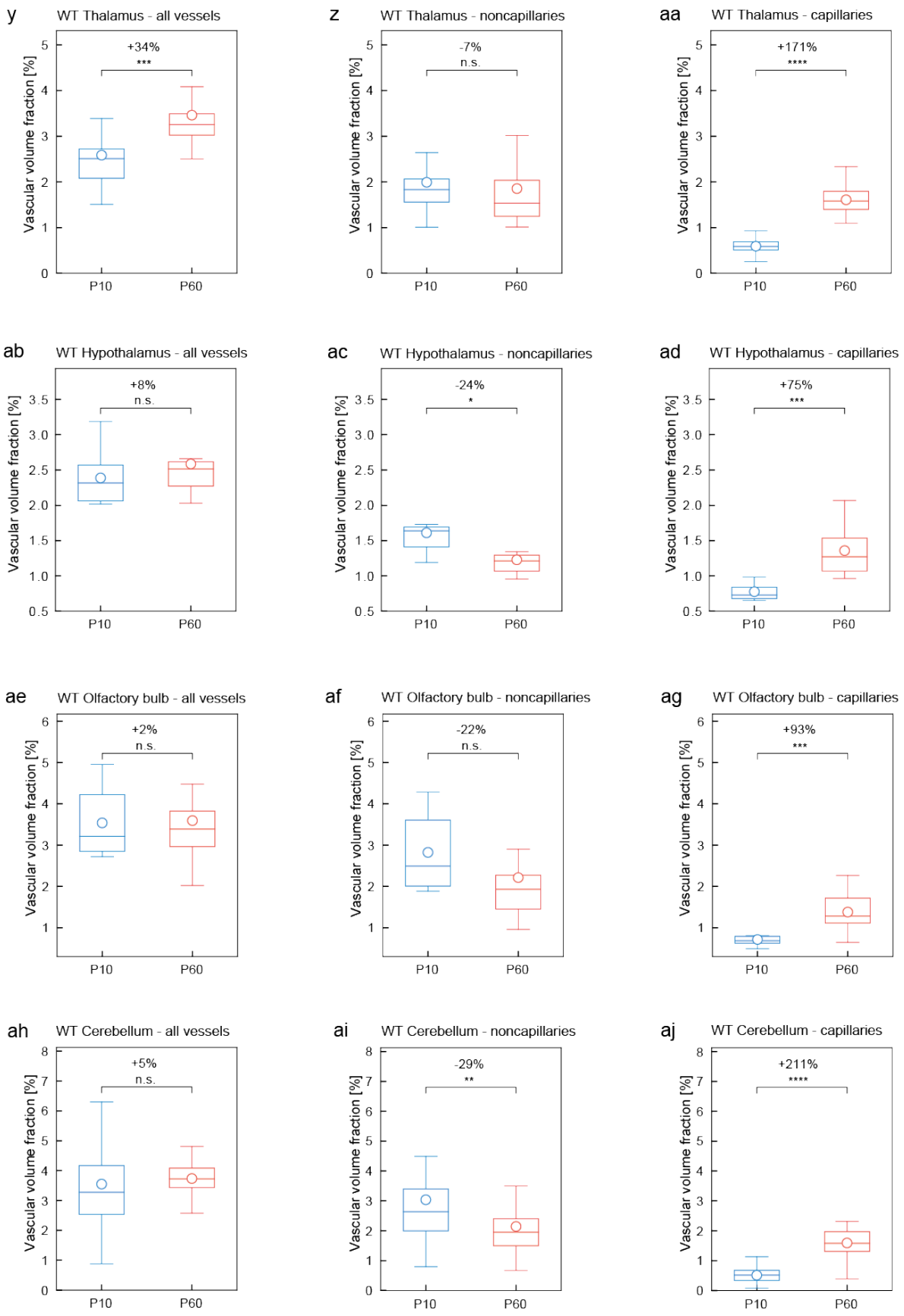

Supplementary Figure 17 continued 3/3

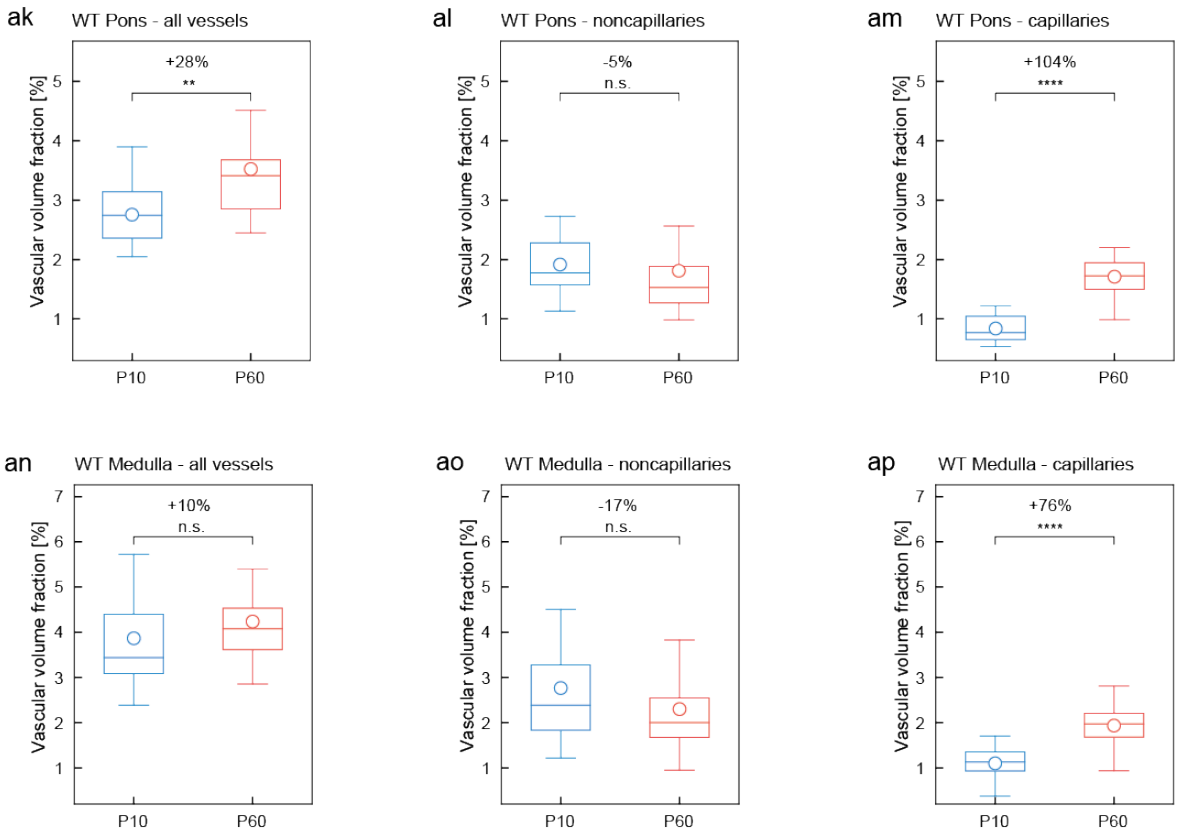

Supplementary Figure 17 Whole-brain scan – local vascular network topology – increased vascular volume fraction of the adult (P60) WT versus postnatal (P10) WT mouse brain mainly found at the capillary level

a-ap Quantification of the 3D vascular volume fraction for all vessels (**a**,**d**,**g**,**j**,**m**,**p**,**s**,**v**,**y**,**ab**,**ae**,**ah**,**ak**,**an**), noncapillaries (**b**,**e**,**h**,**k**,**n**,**q**,**t**,**w**,**z**,**ac**,**af**,**ai**,**al**,**ao**), and capillaries (**c**,**f**,**i**,**l**,**o**,**r**,**u**,**x**,**aa**,**ad**,**ag**,**aj**,**am**,**ap**) in P10 WT and adult (P60) WT mouse brain calculated by local topology analysis in the whole-brain scan. The increase of the vascular volume fraction for all vessels in the P60 WT animals (**a**,**d**,**g**,**m**,**p**,**v**,**y**,**ab**,**ae**,**ah**,**ak**,**an**) was mainly due to a significant increase at the level of capillaries (**c**,**f**,**i**,**l**,**o**,**r**,**u**,**x**,**aa**,**ad**,**ag**,**aj**,**am**,**ap**) in all brain regions (the anatomical regions were divided into ROI-sized section for analysis: between n = 5, dentate gyrus, and n = 126, cortex ROI-sized sections for P10 WT; n = 4, CA3, and n = 76, cortex, ROI-sized sections for P60 WT ROIs were analyzed, highly dependent on the size of the anatomical region). All data are shown

as mean distributions where the open dot represents the mean. Boxplots indicate the 25% to 75% quartiles of the data. *$P < 0.05$, **$P < 0.01$, ***$P < 0.001$.

Supplementary Figure 18

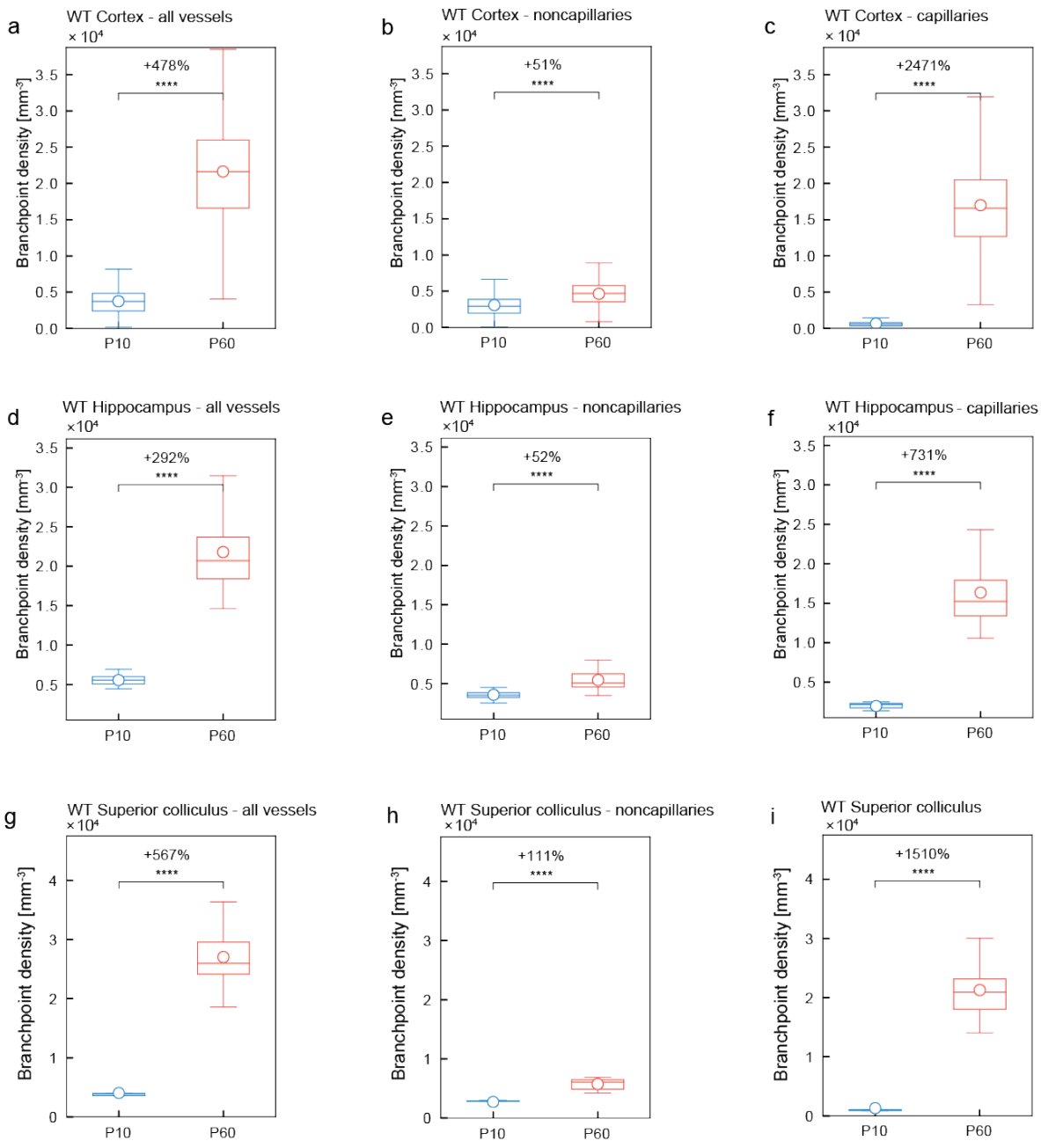

Supplementary Figure 18 Whole-brain scan – local vascular network topology – increased vascular branch point density in various regions of the adult (P60) WT versus the postnatal (P10) WT mouse brain

a-i Quantitative analysis of the branch point density for all vessels (**a**,**d**,**g**), noncapillaries (**b**,**e**,**h**), and capillaries (**c**,**f**,**i**) in the P10 WT and P60 WT mouse brain calculated by local topology analysis in the whole-

brain scan. The significant increase of the branch point density for all vessels in the P60 WT animals (**a**,**d**,**g**) was mainly due to a significant increase at the level of capillaries (**c**,**f**,**i**) and in part due to a significant increase at the level of noncapillaries (**b**,**e**,**h**) (between n = 5, dentate gyrus, and n = 126, cortex ROI-sized sections for P10 WT; and n = 4, CA3, and n = 76, cortex, ROI-sized sections for P60 WT ROIs were analyzed, highly dependent on the size of the anatomical region). All data are shown as mean distributions where the open dot represents the mean. Boxplots indicate the 25% to 75% quartiles of the data. *$P < 0.05$, **$P < 0.01$, ***$P < 0.001$.

Supplementary Figure 19

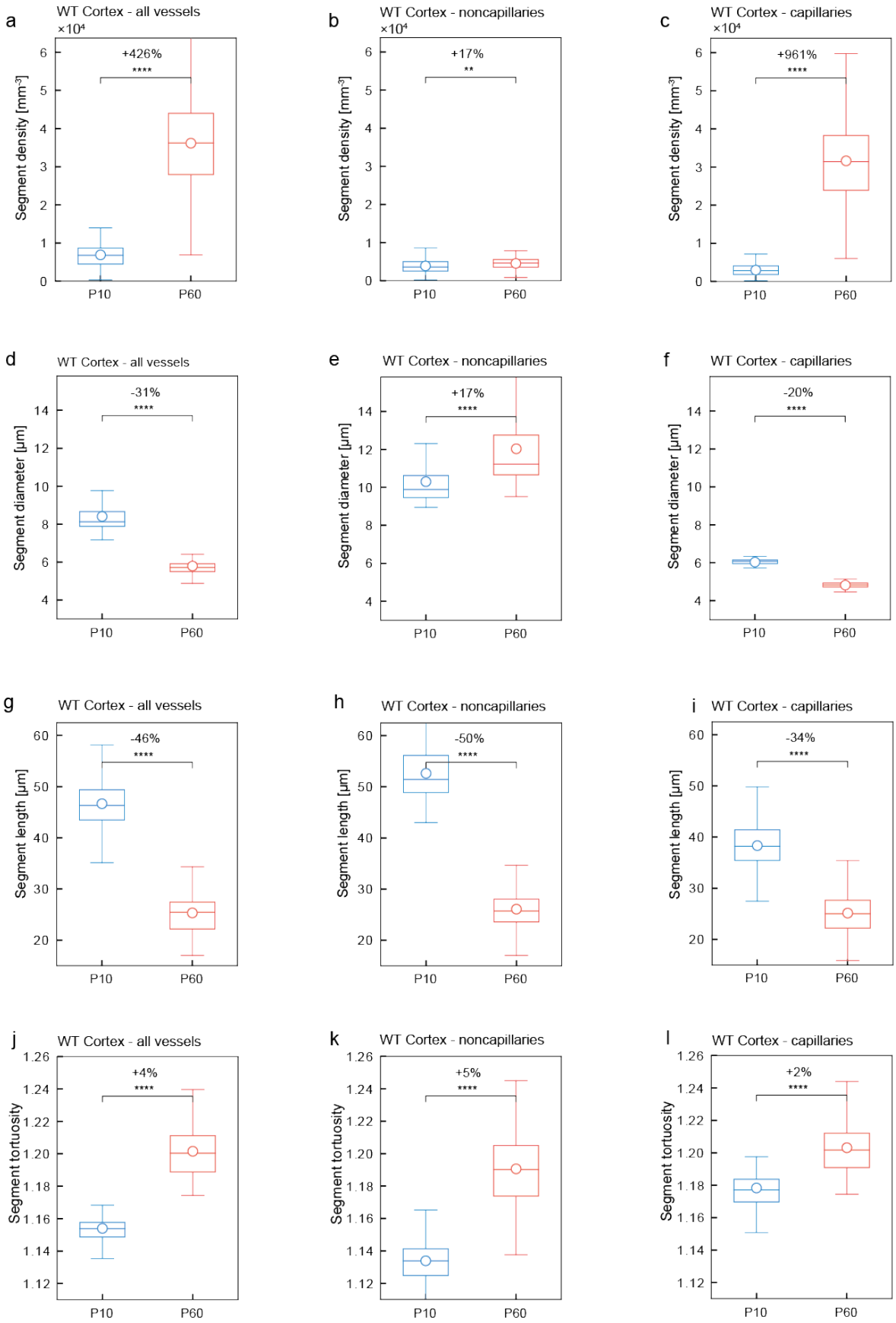

Supplementary Figure 19 continued

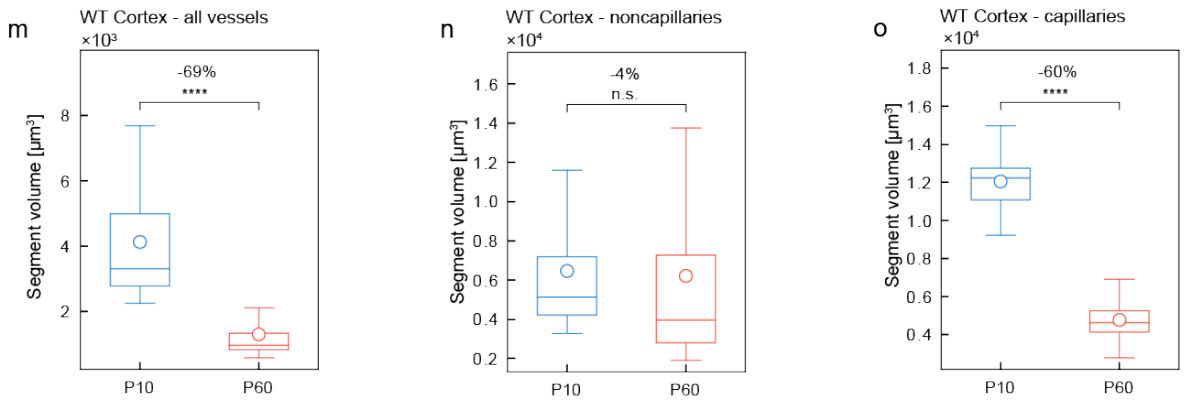

Supplementary Figure 19 Whole-brain scan – local vascular network topology – segment density, diameter, length, tortuosity, and volume of the adult (P60) WT versus the postnatal (P10) WT mouse brain

a-l Quantification of the 3D vessel network parameters segment density (**a-c**), segment diameter (**d-f**), segment length (**g-i**), and segment tortuosity (**j-l**) for all vessels, noncapillaries, and capillaries in P10 WT and P60 WT cortices calculated by local morphometry analysis of the whole-brain scan. The segment density (**a**) and segment tortuosity (**j**) were significantly increased for all vessels in the cortices of P60 WT mice as compared to the P10 WT mice, whereas the segment diameter (**d**) and segment length (**g**) were significantly decreased for all vessels in the P60 WT mice as compared to the P10 WT mice. In line with the other parameters, these differences were mainly due to a highly significant increase respectively decrease at the level of capillaries (**c**,**f**,**i**,**l**) and in part due to an increase respectively decrease at the level of noncapillaries (**b**,**e**,**h**,**k**) (n = 126 ROI-sized sections for the P10 WT cortex; n = 76 for P60 WT cortex were analyzed). All data are shown as mean distributions where the open dot represents the mean. Boxplots indicate the 25% to 75% quartiles of the data. *$P < 0.05$, **$P < 0.01$, ***$P < 0.001$.

Supplementary Figure 20

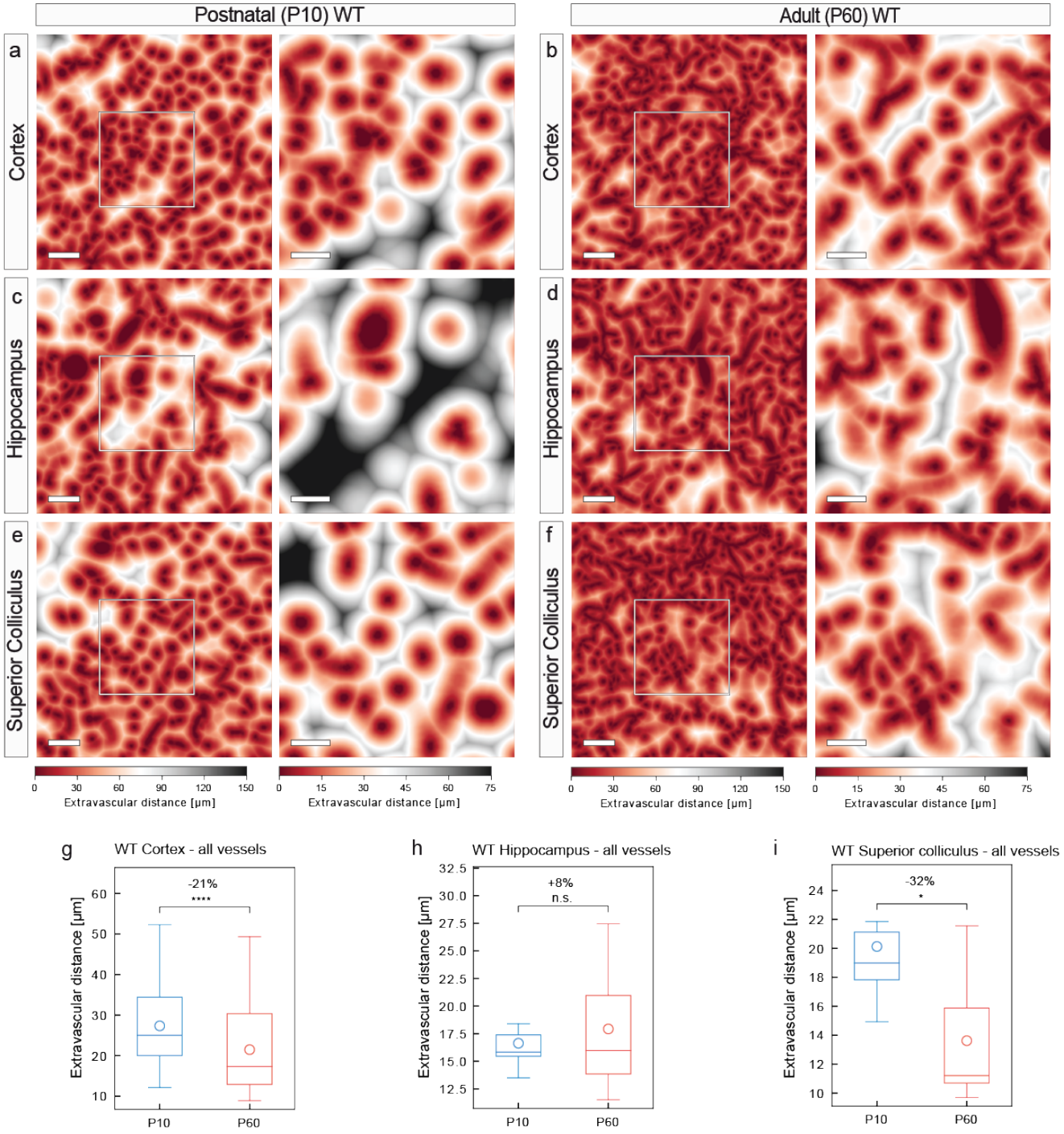

Supplementary Figure 20 Whole-brain scan – local vascular network topology – extravascular distance is decreased in various regions of the adult (P60) WT versus the postnatal (P10) WT mouse brain

a-f Color map indicating the extravascular distance in the cortices, hippocampi and superior colliculi of P10 WT and P60 WT mice. Each voxel outside a vessel structure is assigned a color to depict its shortest distance to the nearest vessel structure. The reduced extravascular distance in P10 WT animals as compared to the P60 WT animals is obvious. The color bar indicates the shortest distance to the next vessel structure. **g-i** Quantification of the extravascular distance in P10 WT and P60 WT in the three brain regions calculated by global morphometry analysis. The extravascular distance in the cortices (**g**), and superior colliculi (**i**) of P60 WT animals was significantly decreased as compared to the P10 WT animals. For the hippocampi (**h**) this difference was not significant (n = 1 for P10 WT; n = 1 for P60 WT animals were used; between n = 5, dentate gyrus, and n = 126, cortex ROI-sized sections for P10 WT; and between n = 4, CA3, and n = 76, cortex, ROI-sized sections for P60 WT ROIs were analyzed, highly dependent on the size of the anatomical region). All data are shown as mean distributions where the open dot represents the mean. Boxplots indicate the 25% to 75% quartiles of the data. *$P < 0.05$, **$P < 0.01$, ***$P < 0.001$.

Supplementary Figure 21

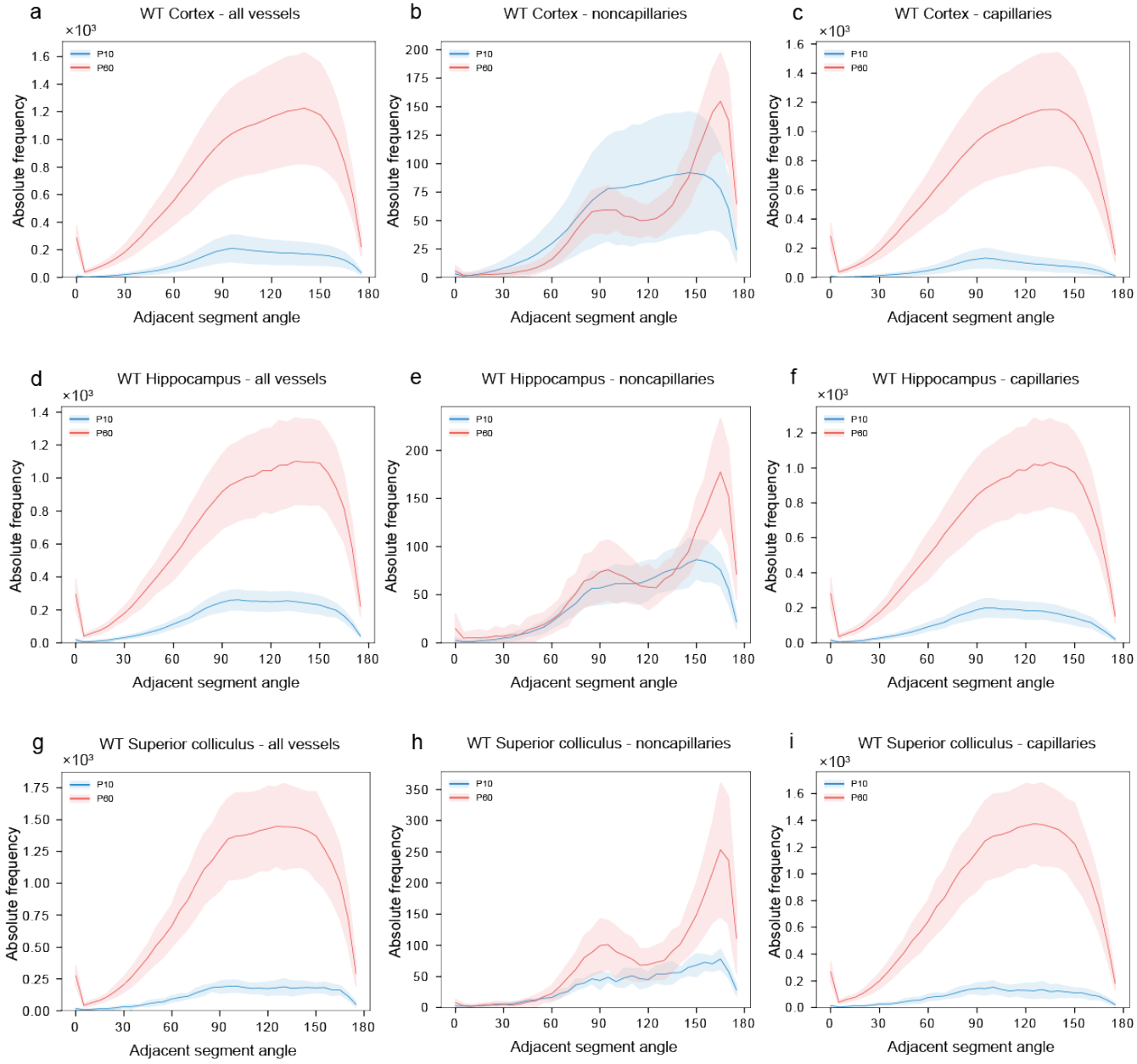

Supplementary Figure 21 Whole-brain scan – Quantification of vessel directionality

Quantitative analysis showing the relative angles of the vascular segments emanating from a certain branch point in the cortex, hippocampus, and superior colliculus on the level of all vessels, noncapillaries and capillaries. **a-i** Analysis revealed that, comparable to the all-vessels group, the capillaries in the cortex, hippocampus, and superior colliculus, derived at angles between around 75° and 150° at both the developing

P10 and mature P60 stages (**c**,**f**,**i**). The noncapillaries, showed two main angles of orientation, namely around 90° and at around 170° in three brain regions examined (**b**,**e**,**h**). These two main angles of orientation were more pronounced at the P60 stage as compared to the P10 stage (**b**,**e**,**h**), and were very similar in the three brain regions, suggesting a more general underlying concept of vessel directionality/orientation. These findings, obtained from the whole-brain scans, show very similar findings to the ROI-based method (see Figure 12) (**a-i** bin width = 5; number of bins = 55).

REFERENCES

1 Todorov, M. I. *et al.* Machine learning analysis of whole mouse brain vasculature. *Nat Methods* **17**, 442-449, doi:10.1038/s41592-020-0792-1 (2020).

2 Walchli, T. *et al.* Quantitative assessment of angiogenesis, perfused blood vessels and endothelial tip cells in the postnatal mouse brain. *Nature protocols* **10**, 53-74, doi:10.1038/nprot.2015.002 (2015).

3 Fantin, A., Vieira, J. M., Plein, A., Maden, C. H. & Ruhrberg, C. The embryonic mouse hindbrain as a qualitative and quantitative model for studying the molecular and cellular mechanisms of angiogenesis. *Nature protocols* **8**, 418-429 (2013).

4 Marinkovic, S., Milisavljevic, M. & Puskas, L. Microvascular anatomy of the hippocampal formation. *Surg Neurol* **37**, 339-349, doi:10.1016/0090-3019(92)90001-4 (1992).

5 Tatu, L. & Vuillier, F. Structure and vascularization of the human hippocampus. *Front Neurol Neurosci* **34**, 18-25, doi:10.1159/000356440 (2014).